Separation and Purification Technology 271 (2021) 118675

Contents lists available at ScienceDirect

Separation and Purification Technology

journal homepage: www.elsevier.com/locate/seppur

P removal from Si by Si-Ca-Al alloying-leaching refining: Effect of Al and the $CaAl_2Si_2$ phase

Mengyi Zhu [a,*], Shengying Yue [b,c,d,*], Guixuan Wu [e,f,*], Kai Tang [g], Yijiang Xu [g], Jafar Safarian [a]

[a] Department of Materials Science and Engineering, Norwegian University of Science and Technology (NTNU), N-7491 Trondheim, Norway
[b] Department of Mechanical Engineering, University of California, Santa Barbara, CA 93106, United States
[c] Aachen Institute for Advanced Study in Computational Engineering Science (AICES), RWTH Aachen University, Schinkelstraße 2, Aachen 52062, Germany
[d] Shandong Institute of Advanced Technology (SDIAT), Shandong University, 250061 Jinan, China
[e] Institute of Energy and Climate Research, Microstructure and Properties of Materials (IEK-2), Forschungszentrum Jülich GmbH, Leo-Brandt-Straße 1, 52425 Jülich, Germany
[f] GTT-Technologies, Kaiserstraße 103, 52134 Herzogenrath, Germany
[g] SINTEF Industry, N-7465 Trondheim, Norway

ARTICLE INFO

Keywords:
Silicon
Phosphorus
Impurity
Segregation
Solidification
Thermodynamics

ABSTRACT

Phosphorus (P) is a critical impurity in metallurgical-grade Si that needed to be removed for solar-grade Si production. The Si-Ca-Al-P system is one of the most crucial alloy systems for Si refining, where P can be separated by either the Si-Al solvent refining or the Si-Ca alloying-leaching process. In this work, a series of Si-Ca-Al alloys were obtained to investigate the role of alloy composition and the $CaAl_2Si_2$ phase in P segregation and separation. The used alumina crucible led to heavy Al contamination and resulted in unexpected Si-Ca-Al alloy compositions. $CaAl_2Si_2$ and $CaSi_2$ were found as the main precipitates, and relatively higher P content was detected in the $CaAl_2Si_2$ phase. Leaching experiments indicate that P removal degree increases with increasing Ca/Al ratio and increasing total alloying amount (Ca + Al). Effects of alloy composition were further analyzed by statistical methods, which indicates Ca firmly plays a strong, positive, and monotonic role in P removal while no strong attraction between Al and P. Theoretical P removal model for the Si-Ca-Al system was established and in good agreement with measured results. Interaction coefficients of Ca and Al to P were fitted as $\varepsilon_{Ca}^{P} = -19.2$ and $\varepsilon_{Al}^{P} = -1.8$, which further confirms Ca is the essential driving force for P segregation. Finally, the possibility of P solid solution formation was verified by first-principle simulations that both $CaAl_2Si_2$ and $CaSi_2$ are able to dissolve P, especially through the Si site, but the $CaAl_2Si_2$ phase is more favourable for P dissolution than $CaSi_2$, which explains the reason of the often detected high P content in $CaAl_2Si_2$.

1. Introduction

Solar energy is a crucial renewable energy source to reduce greenhouse emissions and limits global warming. The strong demand for solar panels is still spreading and expanding faster than ever before. In 2019, a record of 115 GW new solar photovoltaics (PV) capacity was added worldwide for a total of 627 GW, which is more than the summation of all the other renewable power capacity additions [1]. As the dominating feedstock material in the PV industry, solar grade silicon (SoG-Si, purity 99.9999%) has attracted increasing attention globally. Most of the SoG-Si is currently produced by the modified Siemens process and the fluidized bed reactor process. However, both methods are energy-intensive and face the potentially severe environmental issue that the hazardous by-products may leak into the atmosphere, such as chlorinated gases and silane [2]. Thus, the requirement of more sustainable SoG-Si production has encouraged the innovation of more environmentally friendly manufacturing. Many efforts so far have been devoted to refine the metallurgical-grade Si (MG-Si, purity 99%) with lower energy consumption and carbon footprint through the metallurgical techniques like slag refining [3-6], solvent refining [7-13], acid leaching [14-19], vacuum refining [20-23], gas refining [24,25], directional solidification [26], and their combinations [27-30].

* Corresponding authors at: Department of Materials Science and Engineering, Norwegian University of Science and Technology (NTNU), N-7491 Trondheim, Norway (M. Zhu). Shandong Institute of Advanced Technology (SDIAT), Shandong University, 250061 Jinan, China (S. Yue). Institute of Energy and Climate Research, Microstructure and Properties of Materials (IEK-2), Forschungszentrum Jülich GmbH, Leo-Brandt-Straße 1, 52425 Jülich, Germany (G. Wu).
E-mail addresses: mengyi.zhu@ntnu.no (M. Zhu), sheng.ying.yue@rwth-aachen.de (S. Yue), g.wu@fz-juelich.de (G. Wu).

https://doi.org/10.1016/j.seppur.2021.118675
Received 14 December 2020; Received in revised form 14 March 2021; Accepted 22 March 2021
Available online 29 March 2021

According to the nature that most impurities prefer to stay in the liquid phase during silicon solidification, impurities with small segregation coefficients show a strong tendency to gather and form secondary precipitates to be further separated or removed such as Al, Fe, and Ti and so on. However, although P can also segregate along Si grain boundary [31], its relatively large segregation coefficient ($k_P = 0.35$ [32]) still makes it as one of the most critical and problematic impurities to be removed. Thus, the addition of alloying elements is required to enhance its segregation behaviour.

Based on the different alloying concentrations, two different alloying strategies are proposed so far, respectively, solvent refining and Si-alloy based acid leaching (alloying-leaching) technique. Solvent refining requires high concentration alloying of Si to lower the processing temperature and enable the solvation of Si. The Si-Al system is the most investigated solvent with a long history since the 1950s [33], and efficient P removal is reported by many researchers [34-38]. Yoshikawa and Morita [34] observed an inversely proportional relationship between the P segregation coefficient and refining temperature at 1173–1373 K. The main reason for enhanced P removal in the Si-Al was assumed owing to the formation of AlP during solidification [12]. As the formed AlP particle may act as nucleation substrate of Si [39,40], the refining efficiency is significantly affected by thermodynamic and kinetic conditions [36].

In contrast to the solvent refining, the alloying-leaching approach requires minor alloying elements addition that holds strong attraction with the impurities. Ca was firstly employed as an impurity getter by Schei [41] and confirmed with the ability to gather a number of impurities including P. The interaction coefficient between Ca and P in molten Si was determined by Shimpo et al. [14] as a strongly negative value, $\varepsilon_{Ca}^{P} = -14.6 \pm 1.7$ at 1723 K. The strong attraction between Ca and P was further confirmed based on the detection of phosphide formation in a Si- 3 wt% P alloy. Significant P removal enhancement after Ca alloying was also reported by other researchers [16,42-44]. It is also frequently reported that the $CaAl_2Si_2$ phase contains the highest P concentration among all the precipitates. Anglézio et al. [45] found that $CaAl_2Si_2$ is the only phase contains P in MG-Si with 0.22 wt% Ca, 0.18 wt % Al, and 0.31 wt% Fe. Margaria et al. [46] reported that the P content in $CaAl_2Si_2$ phase in an industrial MG-Si (98.5 wt% Si, 0.6 wt% Ca, 0.4 wt% Al, and 0.3 wt% Fe) could reach as high as 1 wt% and usually may contain more than half of the total P content. Moreover, the $CaAl_2Si_2$ phase was also detected with high P concentration in the Ca alloyed Si. In the study of Hu et al. [47], P removal significantly increased after Ca alloying and the reason was linked to the increase of $CaAl_2Si_2$ phase. In the directional solidification study of a Si- 30at% Al, the P enrichment in $CaAl_2Si_2$ phase was also observed by Sun et al. [48] even with low Ca content. It was further deduced that the less compacted crystal structure of $CaAl_2Si_2$ may favour P dissolution. With the purpose to study the P removal by $CaAl_2Si_2$ phase formation, Lai et al. [49] studied the alloying-leaching process of a Si-6.7at% Al-3.3at% Ca alloy, P signal was observed in the obtained $CaAl_2Si_2$ phase by EPMA detection, and a final 87% P removal was achieved. Recently, P enrichment in the $CaAl_2Si_2$ phase was also observed by Zhang et al. [50] through a novel slag refining and Si-Ca-Al solvent refining combined process.

Although the $CaAl_2Si_2$ phase has been widely detected with high P content, it still remains uncertain about the P segregation's compositional dependence in the Si-Ca-Al-P system. This work aims to assess how P segregation is affected by the Si-Ca-Al alloy concentration and the formation of the $CaAl_2Si_2$ phase. In addition, the effect of commonly used alumina crucible is also discussed as it was later found to contaminate all Ca-containing alloys and resulted in unexpected high Al concentration. The contributions of Ca and Al concentration on P removal were further studied through statistical methods. An analytical model for P removal in the Si-Ca-Al system was established to quantify the effect of Ca and Al concentration on the alloying-leaching process. Moreover, first-principle calculations were also applied to assess the possibility of P solid solution formation in the two common precipitates, $CaAl_2Si_2$ and $CaSi_2$.

Table 1
Initial charged alloy composition and materials.

Sample	Initial charged composition (wt%)		Initial charged mass of materials into alumina crucible (g)		
	Ca	Al	MG-Si	Ca	Al
A	4.0	–	11.52	0.48	–
B	4.3	–	11.49	0.51	–
C	4.7	–	11.46	0.56	–
D	5.4	–	11.36	0.66	–
E	4.0	0.2	11.50	0.48	0.03
F	4.0	0.5	11.47	0.48	0.07
G	4.0	1.0	11.41	0.48	0.11

2. Methodology

2.1. Experimental

Commercial MG-Si was employed as the starting material. The specific amount of Ca granules (99% purity, Sigma-Aldrich) and Al chips (99.99% purity, Hydro AS Norway) were mixed with MG-Si lumps in Alsint alumina crucible (99.7% purity, inner diameter: 2.6 cm, outer diameter: 3 cm, height: 4 cm) and with a total amount fixed at around 12 g (Table 1). The alumina crucibles were placed inside a highly dense graphite crucible and put into an induction furnace. Before heating, the furnace was evacuated to 10^{-1} mbar and refilled to 1 bar with continuous high purity Ar flow (+99.999% purity). Crucibles were later on heated to 1500 °C and held for 10 min to make sure the sample is completely melted and homogenized by the electromagnetic force induced stirring. The molten alloys were then slowly cooled down to room temperature inside the furnace by an average cooling rate around 10 °C/min. Subsequently, solidified samples contain alloy-crucible interface and large particles (over 5 mm) from the bulk alloy were collected and prepared for microstructural analysis by Electron Probe Micro-Analyzer (EPMA, JXA-8500F). The surface of remained bulk samples were then mildly grinded to remove the adjacent pieces of crucible fragment, and then crushed and milled to specific particle sizes (0.1–0.6 mm) for the following acid leaching process.

In the leaching trials, 2 g of the sized samples were charged into a perfluoroalkoxy (PFA) bottle with 10 mL 10% HCl and then placed in an ultrasonic bath at 60 °C for 2 h. After leaching, the samples were washed by ethanol three times and dried inside the drying oven. The chemical compositions of the all samples were measured by high resolution Inductively Coupled Plasma-Mass Spectroscopy (ICP-MS, Thermo Scientific Element 2, US).

2.2. Computational simulation

First-principle calculations based on the density functional theory (DFT) were performed to further analyse the experimental results. In the simulation, the possibility of P solid solution formation in the two precipitated phases $CaAl_2Si_2$ and $CaSi_2$ was investigated by adopting a $2 \times 2 \times 3$ unit cell as supercell. Accordingly, 60 and 36 atoms were set in the supercell of each case. We performed the first-principles code Vienna Ab-initio Simulation Package (VASP) [51,52]. The adopted pseudopotentials are based on the projector augmented wave (PAW) method [53] from the VASP library with the generalized gradient approximation by Perdew, Burke, and Ernzehof (GGA-PBE) [54]. The energy cutoff of a plane wave kinetic is 800 eV [55]. The Monkhorst-Pack k-point mesh of $9 \times 9 \times 3$ was found to be enough to converge the total energy up to 5 meV. The energy cutoff of augmented plane waves was checked to ensure the convergence. Full optimizations were applied to both structures with the Hellmann-Feynman forces tolerance 0.0001eV/Å. The total energy and the enthalpy of P substituted $CaAl_2Si_2$ and $CaSi_2$ was calculated via static DFT calculations.

Table 2
Measured composition of the obtained Si-Ca-Al alloys presented in the units of ppmw and ppma. For each sample, the upper row indicates the unit of ppmw, and the bottom row indicates the unit of ppma and in parenthesis.

Sample	Composition of obtained alloys ppmw/(ppma)							
	P	Ca	Al	Fe	Ti	Si	Ca/Al	Ca + Al(%)
A	14.5	33,899	8213	2820	249	Bal.	4.1	4.2
	(13.3)	(24028)	(8648)	(1435)	(148)	(Bal.)	2.8	3.3
B	16.8	15,824	21,874	2996	264	Bal.	0.7	3.8
	(15.4)	(11147)	(22897)	(1515)	(156)	(Bal.)	0.5	3.4
C	15.6	16,368	18,588	2221	202	Bal.	0.9	3.5
	(14.2)	(11532)	(19455)	(1123)	(119)	(Bal.)	0.6	3.1
D	13.0	44,489	14,906	2843	267	Bal.	3.0	5.9
	(12.0)	(31627)	(15741)	(1450)	(159)	(Bal.)	2.0	4.7
E	13.7	30,448	11,900	2946	270	Bal.	2.6	4.2
	(12.6)	(21558)	(12516)	(1497)	(160)	(Bal.)	1.7	3.4
F	12.3	29,346	9725	2572	232	Bal.	3.0	3.9
	(11.3)	(20768)	(10224)	(1306)	(137)	(Bal.)	2.0	3.1
G	13.5	23,630	27,127	3122	273	Bal.	0.9	5.1
	(12.4)	(16687)	(28458)	(1582)	(162)	(Bal.)	0.6	4.5

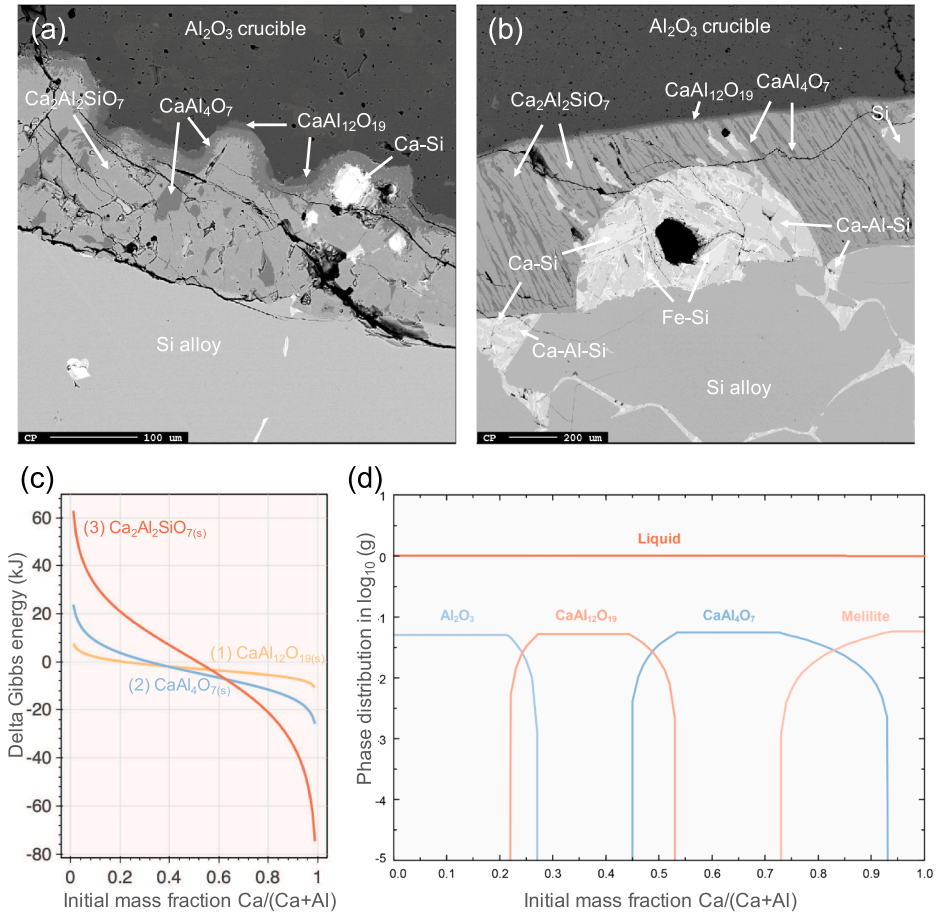

Fig. 1. Backscatter image of the interface microstructure between Al_2O_3 crucible and Si-Ca-Al alloy (a) Ca-higher sample; (b) Al-higher sample; (c) Composition dependence of delta Gibbs energy of possible reactions at 1500 °C where the solution state was assigned for the metal phase in the FTlite database, and the most stable solid state was assigned for each oxide in the FToxid database; (d) Local equilibrium between 95 wt% Si-Ca-Al alloy (1 g) and Al_2O_3 (0.05 g) with varying Ca and Al concentration at 1500 °C.

3. Results and discussion

3.1. Interaction of melt with alumina crucible

The compositions of obtained alloys are measured by ICP-MS and listed in Table 2. It was found that in all the alloys, the Al concentration is much higher than the initial charged, which indicates that the reactive Si-Ca melt was corrosive to the Al_2O_3 crucible, thus, all the alloys were contaminated. Similar contamination effect was also reported by Sakiani et al. [56]. It is also worth noting that since the initial charged alloy compositions had changed, all the impurity removal analyses below are based on the final measured ternary Si-Ca-Al alloy compositions as listed in Table 2.

As the alloys underwent heavy contamination, it is thus necessary to examine the interaction between alloyed Si melt and Al_2O_3 crucible. According to the different contamination levels, sample A (Ca-higher, slightly contaminated) and sample G (Al-higher, heavily contaminated) are selected as the representative samples. Backscattered electron images are shown in Fig. 1(a) and (b) along the alloy-crucible interface of, respectively, sample A and sample G, and revealed the formation of different slag layers.

Firstly, it is seen that the formed slag layers are with different

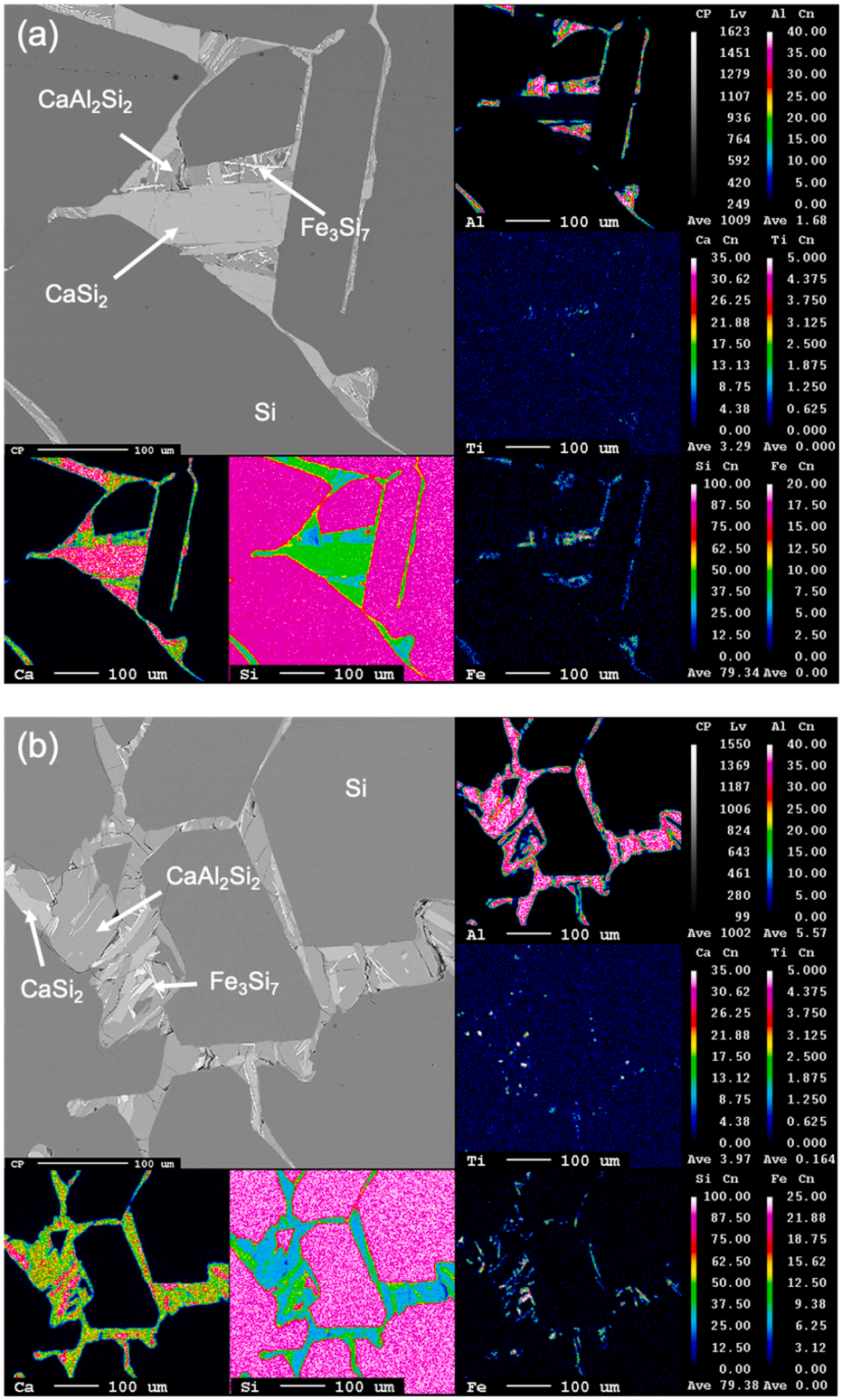

Fig. 2. EPMA elemental mapping of the microstructure of Si-Ca-Al alloy (a) sample A (Ca-higher); (b) sample G (Al-higher).

thicknesses. In sample A, as shown in Fig. 1(a), the thickness of the slag layer is only around 100 μm, but in the heavily contaminated sample G, the thickness significantly increases to around 700 μm (Fig. 1(b)), which indicates a large amount of Ca loss and Al substitution from the crucible. Additionally, in Fig. 1(b), it still can be seen that several Ca-Si and Ca-Al-Si phases stay close to the crucible interface as evidence of a series of complex reactions.

The composition of observed slag phases was further measured by point analysis of wavelength-dispersive spectrometer equipped in the EPMA, and determined as $CaAl_{12}O_{19}$, $CaAl_4O_7$, and $Ca_2Al_2SiO_7$ as shown in Fig. 1(a) and (b). Thus, the formation of the slag layers may be represented by the reactions as follows:

$$\frac{3}{19}\underline{Ca} + Al_2O_{3(s)} = \frac{3}{19}CaAl_{12}O_{19(s)} + \frac{2}{19}\underline{Al} \quad (1)$$

Table 3
Measured composition of major phases in sample A (Ca-higher) and sample G (Al-higher) in at%.

Sample	Phase	Si	Ca	Al	Fe	Ti	P
Sample A (Ca-higher)	Si	99.4	0.1	0.3	0.05	0.06	0.0009
	$CaSi_2$	66	33	1.1	0.04	–	0.01
	$CaAl_2Si_2$	42	20	38	0.06	0.005	0.06
	Fe_3Si_7	67	0.3	5.8	27	0.04	0.02
	Fe-Ti-Al-Si	42	0.9	18	21	18	–
Sample G (Al-higher)	Si	99.6	0.1	0.4	0.02	–	–
	$CaSi_2$	65	34	1.1	0.1	–	0.009
	$CaAl_2Si_2$	41	22	37	0.04	0.02	0.01
	Fe_3Si_7	67	0.3	5.1	28	0.0009	0.002

$$\frac{3}{7}\underline{Ca} + Al_2O_{3(s)} = \frac{3}{7}CaAl_4O_{7(s)} + \frac{2}{7}\underline{Al} \quad (2)$$

$$\frac{6}{7}\underline{Ca} + \frac{3}{7}\underline{Si} + Al_2O_{3(s)} = \frac{3}{7}Ca_2Al_2SiO_{7(s)} + \frac{8}{7}\underline{Al} \quad (3)$$

To further understand the effect of initial charged alloy composition (Ca/Ca + Al) on the melt-crucible interaction, Factsage™ 7.3 with the commercial databases FTlite and FToxid was applied to calculate the Gibbs energy change of above equations and the local equilibrium result with fixed Si content at 95 wt% at 1500 °C. In the calculation, solution state was assigned for the metals, and the most stable solid state was assigned for the oxides. As shown in Fig. 1(c) and (d), it is seen that the above aluminates prefer to form at different composition region where $Ca_2Al_2SiO_7$ is preferable to form in Ca-higher alloy and with lowering Ca/(Ca + Al) ratio, the formation of $CaAl_4O_7$ and $CaAl_{12}O_{19}$ appears. The calculation is also in agreement with the observed samples. For example, for the sample A shown in Fig. 1(a), which is an initially charged Si-Ca binary alloy with the Ca/Ca + Al ratio equals to 1, the $Ca_2Al_2SiO_7$ phase, i.e. Melilite, is observed as the dominant slag layer, and the $CaAl_4O_7$ and $CaAl_{12}O_{19}$ phases are seen in the thin layer closer to Al_2O_3 due to the uneven distribution of consuming Ca and substituting Al in the infiltration front. For the sample G shown in Fig. 1 (b), which is an initially charged Si-Ca-Al ternary alloy with the Ca/Ca + Al ratio equals to 0.8, eutectic pattern between $Ca_2Al_2SiO_7$ and $CaAl_4O_7$ is observed as clearly indicated in Fig. 1(d).

As the interaction between alumina crucible and Si-Ca-Al melt exist in a wide composition range, it is concluded that alumina crucible is not suitable to hold the Si-Ca and Si-Ca-Al melt considering of the consumption of Ca and contamination of Al substitution from the crucible.

3.2. *Effect of Ca/Al ratio on microstructure*

The microstructure evolution and impurity distribution with varying Ca/Al mixing ratio were characterized by EPMA elemental mapping analysis and typical results are presented in Fig. 2. The detected main phases are listed in Table 3. It is seen that the Ca/Al mixing ratio plays a vital role in the alloy microstructure. In both Ca-higher and Al-higher Si-Ca-Al alloys, $CaSi_2$ and $CaAl_2Si_2$ phases are observed as the common phase but with different fractions, while the $CaAl_2Si_2$ phase in each sample was detected with the highest P content, even though the values might be not fully reliable due to the low P amount and the detection limit even after calibration. In the Ca-higher sample, as presented in Fig. 2(a), the amount of $CaSi_2$ phase is higher than that of $CaAl_2Si_2$, while in the Al-higher alloy, as shown in Fig. 2(b), the ternary compound $CaAl_2Si_2$ becomes the dominant precipitate as the measured Ca/Al mole ratio is close to 0.5. However, it is worth noting that since the P concentration is lower than the detection limit even after calibration, the distribution of P cannot be directly observed. The transition metal impurities Fe and Ti are found appearing in two kinds of precipitates, which are with the detected stoichiometry of Fe_3Si_7 and a novel quaternary Al-Fe-Ti-Si phase with a detected stoichiometry as $AlFeTiSi_2$. It is worth noting that even though the Fe_3Si_7 phase (also known as high-temperature $FeSi_2$ phase, $FeSi_{2.4}$ and α-leboite) could be stabilized by Al impurity down to room temperature [57], it is also possible that some minor portion of decomposition product $FeSi_2$ and Si exit but cannot be identified due to their ultrafine size and the slow solid–solid decompose reaction that makes them not fully separated. The Ti-bearing phase is always fine particles and adjacent the Fe-bearing phase. Interestingly, it is observed that, in all the observed Si-Ca-Al

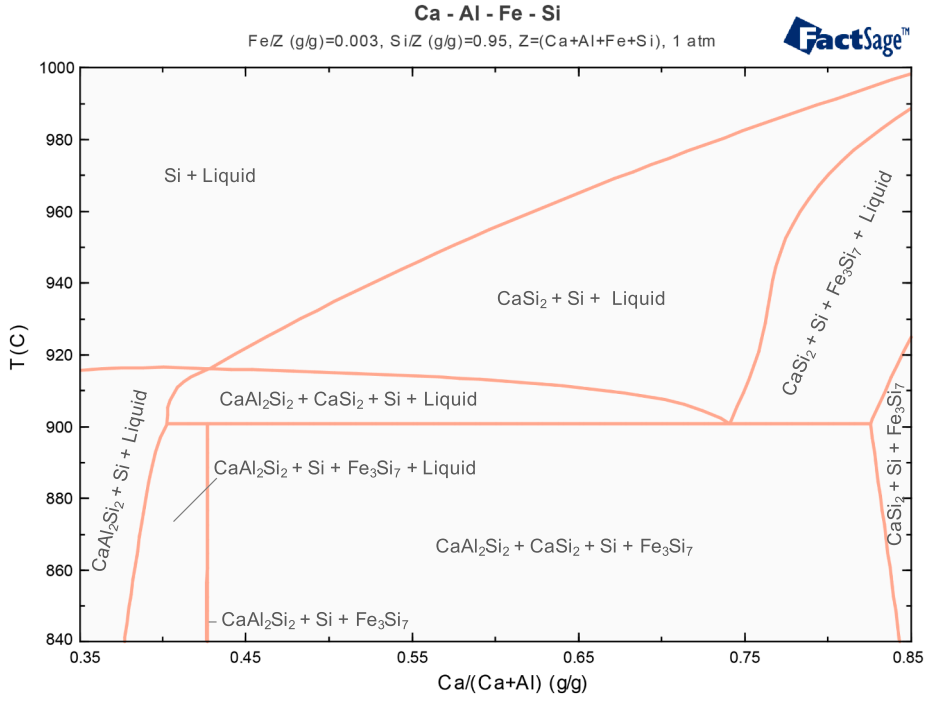

Fig. 3. Calculated Ca-Al-Fe-Si quaternary phase diagram with 95 wt% Si, 3000 ppmw Fe, and varying Ca/Al ratio.

alloys, the transition metal impurities are all embedded inside the $CaAl_2Si_2$ phase instead of $CaSi_2$. To further investigate the phenomenon, the Ca-Al-Fe-Si quaternary phase diagram was plotted by fixing at 95 wt% Si and 3000 ppmw Fe, and with varying Ca/Al ratio, as shown in Fig. 3. This phase diagram was calculated by FactSage 7.3 using FTlite database with setting $FeSi_2$ and its corresponding solution phase as dormant phase due to the presence of the aforementioned Fe_3Si_7 (α-leboite) at room temperature under the present experimental condition. It is seen in the majority of composition range, $CaSi_2$ phase precipitates ahead of the $CaAl_2Si_2$ phase and the Fe_3Si_7 phase. Moreover, a wide eutectic region exists and indicates that $CaAl_2Si_2$ phase and Fe_3Si_7 phase are likely to form together. Thus, the $CaAl_2Si_2$ phase was found as the impurity gathering phase of transition metals.

3.3. Phosphorus removal in leaching

In the acid leaching process of Si-Ca-Al alloy, the precipitated main silicide phases like $CaSi_2$ and $CaAl_2Si_2$ readily dissolve into the acidic solution, consequently, the embedded P impurity is carried away and removed. The probable leaching reactions can be written as [58,59]:

$$(CaSi_2)_n + 2nHCl + xnH_2O \rightarrow \left(Si_2H_{2-x}(OH)_x\right)_n + nCaCl_2 + xnH_2(g)\,(0 \le x \le 2) \quad (4)$$

And,

$$CaAl_2Si_2 + 8HCl \rightarrow 2AlCl_3 + CaCl_2 + 2SiH_2(g) + 2H_2(g) \quad (5)$$

The calculation of P removal degree is shown below:

$$\eta = \frac{(X_{final} - X_{initial})}{X_{initial}} \times 100\% \quad (6)$$

where X_{final} denotes the P content in purified Si after leaching and $X_{initial}$ denotes the initial P content before leaching listed in Table 2 in ppma.

The results of the P removal degree of the studied Si-Ca-Al alloys after leaching are presented in Fig. 4. It is seen that when the Ca/Al ratio close to 0.5, the P removal degree increases from 64.7% to 77.7% with the increment of total Ca and Al alloying concentration, which improves from 3.1 mol% to 4.5 mol%. A similar trend can also be observed for the alloys with Ca/Al close to 2.0, where the P removal degree increases from 71.9% with 3.1 mol% Ca and Al alloying mole concentration to 86.0% with (Ca + Al) mol% equals 4.7 mol%. Moreover, it can also be observed that with similar Ca and Al total alloying concentration, the alloys with a higher Ca/Al ratio always exhibiting higher P removal with no matter that how much is the total (Ca + Al) alloying concentration.

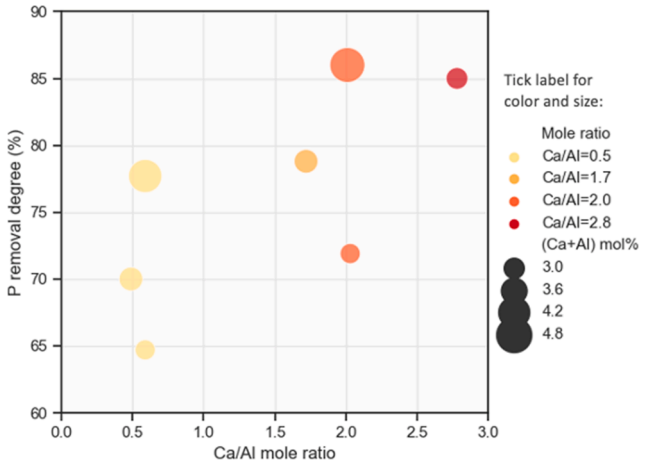

Fig. 4. Measured P removal degree of studied Si-Ca-Al alloys where the size of the dots indicates the total alloying concentration of Ca and Al, and the different color of the dots indicate different Ca/Al mole ratio.

For instance, the P removal degree increases from 70.0% to 78.8%, with the Ca/Al ratio increases from 0.5 to 1.7, while the (Ca + Al) mol% amount in both alloys is equal to 3.4. Moreover, the P removal degree further rises to 85.0%, with the Ca/Al ratio increases to 2.8. Thus, above all, two clear trends can be summarized: 1) P removal degree increases with increasing total amount of Ca and Al, 2) P removal degree increases with increasing Ca/Al mixing ratio.

Interestingly, even though $CaAl_2Si_2$ becomes the major precipitate when Ca/Al is close to 0.5, and frequently found with relatively higher P content by EPMA, however, the present purification results suggest that P removal is enhanced more likely due to increasing Ca addition. Thus, the role of Al and $CaAl_2Si_2$ is discussed in the following sections.

3.4. Correlation analysis

Correlation analysis offers a direct statistic perspective on whether or not two bivariate variables are related. Thus, how well the relationship between initial alloy composition and the final P removal degree can be assessed and described by the correlation coefficient, which constrains between −1 and 1. Pearson's correlation and Spearman's correlation are the two most widely used statistic measures for the study of the correlated relationship between paired data. However, Pearson's correlation only measures the strength of the linear relationship between paired variables and requires normal distribution of the variables, but Spearman's correlation is based on the statistic dependence between the rankings of two variables and therefore works for the non-linear relationship. Thus, Spearman's correlation is selected in this work, considering the complexity of the non-linear relationship between the factors.

The calculation of Spearman's correlation is according to the formula below:

$$r_s = 1 - \frac{6\sum d_i^2}{n(n^2-1)} \quad (7)$$

where n is the number of observations and d_i is the difference between paired ranks (r): $d_i = r_{x_i} - r_{y_i}$.

The results of the calculated Spearman's correlation coefficient (r_s) and corresponding significance testing values (p) are presented in Fig. 5 and Table 4. Apparently, a strong, positive, and monotonic correlation between Ca concentration and final P removal degree ($r_s = 0.93$, $n = 7$, $p < 0.005$) can be seen, which demonstrates the strong P attraction ability of Ca during the solidification process. However, the Al concentration and P removal degree shows a moderate negative relationship but maybe without the statistical significance of monotonic association since the p-values fall beyond the criteria 0.005 ($r_s = -0.43$, $n = 7$, $p > 0.005$). The result also suggests that the role of Al concentration in P separation might be more complicated than merely positive or negative. Taking into account the correlation between the concentration of the elements in alloys, it can be found that Fe and Ti are with a certain strong, positive, and monotonic relationship ($r_s = 0.89$, $n = 7$, $p < 0.005$). This also demonstrates the fact that transition metal impurities Fe and Ti are with strong cohesive properties to form an intermetallic or solid solution. In addition, as expected, the correlation coefficient between Ca and Al concentration exhibits a strong negative value ($r_s = -0.64$, $n = 7$, $p > 0.005$), which indicates the substitution reaction between Ca and Al_2O_3. However, the failed significance test is also apparent since parts of Al were artificially added for the alloying.

It is seen that most of the paired variables did not pass the significance testing, which makes the obtained correlation coefficient remains uncertainty. To further investigate the relationship between the P removal degree and initial alloy composition, the bootstrap sampling method was applied to offer the statistical inference of 95% confidence interval of the Spearman's correlation.

The bootstrap sampling method is a random drawing process with reposition from the existing dataset, which is a powerful apporach to estimate statistical properties and particularly feasible for small size

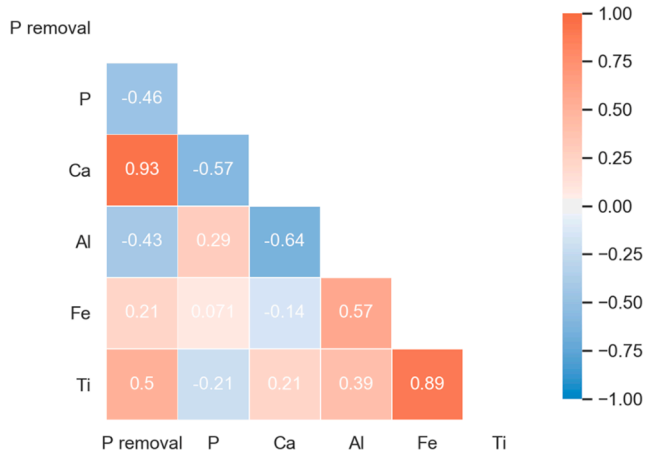

Fig. 5. Results of Spearman correlation analysis between final P removal degree and the concentration of P, Ca, Al, Fe, and Ti before leaching.

Table 4
Significance testing results of monotonic relationship where the "*" in the superscript highlights the p-value smaller than the criteria 0.05.

	P removal	P	Ca	Al	Fe	Ti
P removal	–					
P	0.29	–				
Ca	0.003*	0.18	–			
Al	0.34	0.54	0.12	–		
Fe	0.64	0.88	0.76	0.18	–	
Ti	0.25	0.64	0.64	0.38	0.007*	–

datasets. Accordingly, it was applied for the Spearman's correlation calculation of the total dataset of 7 alloys. Totally 10,000 bootstrap replicate samples were generated based on the random drawing process with reposition from the initial 7 datasets. Each bootstrapped dataset also contains 7 alloys but may not identical to the original dataset due to the random drawing nature. Finally, Spearman's correlation was calculated for the 10,000 bootstrapped samples, and the distribution of

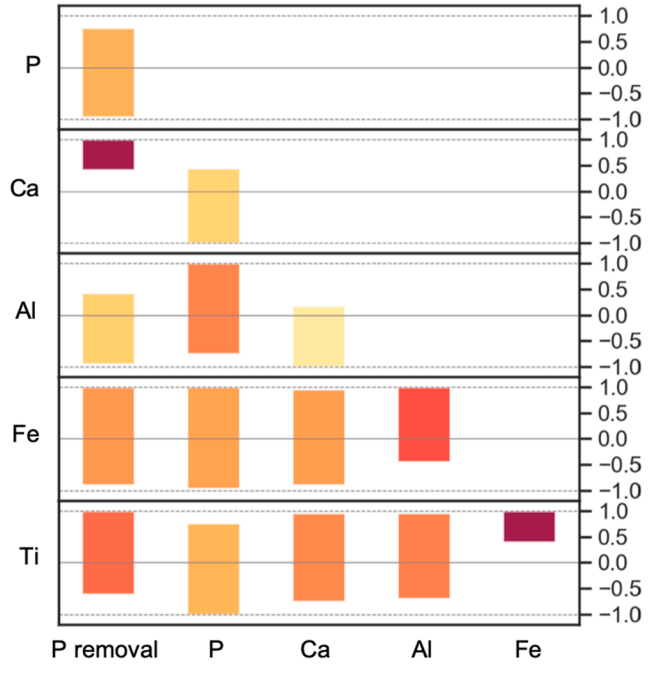

Fig. 6. Spearman's correlation coefficient with 95% confidence interval by 10000-times bootstrap sampling.

Table 5
Projection of variance explained by latent factor.

Latent factor	X variance	Cumulative X variance	Y variance	Cumulative Y variance
1	0.75	0.75	0.64	0.64
2	0.25	1.00	0.15	0.79

Table 6
Variable importance in the projection.

Variables	Latent factors	
	1	2
Ca	1.32	1.25
Al	0.52	0.69

the correlation coefficient is obtained.

Fig. 6 presents the 95% confidence interval of Spearman's correlation of each paired variable. It is seen that the interval between P removal and Ca alloying concentration ranges from 0.41 to 1.00, which confirms the strongly positive and monotonic role of Ca played for P removal with 95% confidence. Meanwhile, the 95% confidence interval between Al concentration and P removal changes from −0.93 to 0.43. Thus, it can be concluded that Al does not play a significant positive role in the P removal in the alloying-leaching process. In addition, the interval between Ca and Al is in the range −1.00 to 0.18, which also offers evidence of the substitution reaction between Ca and the alumina crucible. The strong relationship between Fe and Ti also is confirmed by the bootstrap sampling with the correlation coefficient interval varies from 0.40 to 1.00. This positive interval also offers a hint that the two impurities appear in the same phase in the raw MG-Si.

As a short summary of the statistical analysis, a strong and positive relationship between Ca addition and P removal is confirmed while the attraction between Al-P is suggested not significant.

3.5. Partial least square regression

Partial least square regression (PLSR) is a predictive algorithm that bears the features of principal component analysis and multiple regression, which is particularly useful to handle the variables with high collinearity and reveal the contribution of each variable from different dimensions. The basic algorithm of PLSR is deriving latent factors, which are optimal linear combinations of the variables of the regressed datasets. The general expression of multivariate PLSR is written as below:

$$X = TP^T + E \tag{8}$$

$$Y = UQ^T + F \tag{9}$$

where X is an $n \times p$ matrix of independent variables and Y is an $n \times q$ matrix of dependent variables, the decomposition of X and Y are made to maximize the covariance of T and U, which are two $n \times l$ matrices as the projections of X and Y. P and Q are $p \times l$ and $q \times l$ orthogonal loading matrices, respectively, while the remaining E and F are error terms.

To study the relations between P removal degree and initial concentration of Ca and Al, PLSR becomes a useful tool since the collinearity issue exists due to the substitution reaction between Ca and Al in this work. More specifically, PLSR also facilities the seeking of potential fundamental relations between alloy compositions and P segregation.

The projection of variance explained by latent factors is listed in Table 5. It can be seen that the first latent factor can explain 64% information from the dependent variables, the P removal degree, and in total, 79% of the information of the dependent variable can be explained by the two latent factors where is acceptable for the further calculation. Table 6 lists the variable importance in the projection (VIP), which

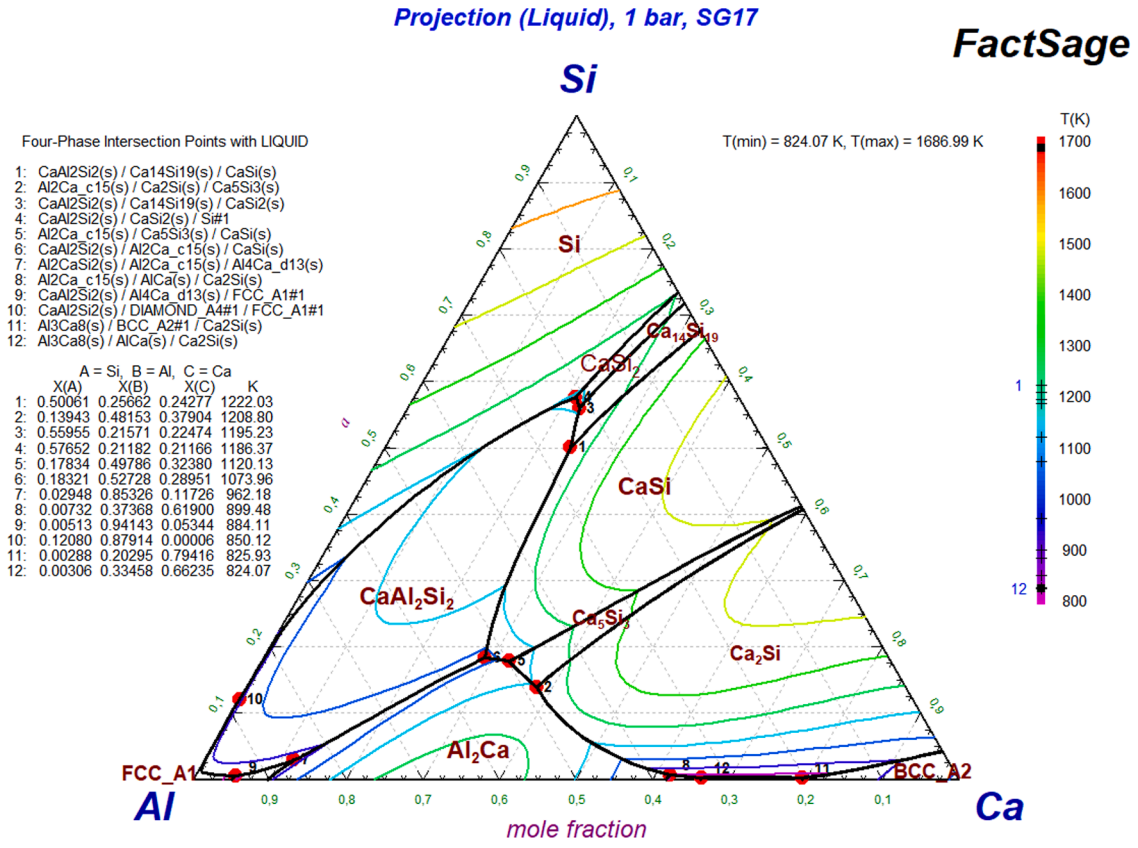

Fig. 7. Liquidus project of Si-Ca-Al alloy system.

measures the importance of variables on the explanation of the latent factor. It is seen that the VIP values of Ca concentration are bigger than 1 in both latent factors, which qualitatively indicates that Ca plays a more important role than that of Al in the P removal.

Furthermore, the regression results using the two latent factors is obtained as:

$$\eta_P{}^* = 0.68t_1 + 0.54t_2 \tag{10}$$

where $\eta_P{}^*$ is the standardized value of the P removal degree. t_1 and t_2 are the obtained latent factors that explain most of the information about the variables and can be further expressed as:

$$t_1 = 0.93x_{Ca}{}^* - 0.37x_{Al}{}^* \tag{11}$$

$$t_2 = 0.64x_{Ca}{}^* + 0.82x_{Al}{}^* \tag{12}$$

where $x_{Ca}{}^*$ and $x_{Al}{}^*$ are standardized concentration of Ca and Al.

Since the obtained latent factors by PLSR cover the dominant information of variables and are explainable, the two latent factors reflect the nature that P segregation is governed from two perspectives, which are the chemical attraction from other elements (t_1) and the physical effect of solidification (t_2). The chemical term t_1 can be linked to the Ca/Al ratio as the fitting parameters show good agreement with the P removal results presented in Fig. 4 that with increasing Ca/Al ratio, the P removal degree increases. It can be seen that Ca contributes positively to the P attraction with the coefficient 0.93, while Al plays a negative role with the coefficient −0.37, which indicates with a fixed total alloying amount, Al substitution for Ca weakens the overall attraction of P chemically. For the physical term, t_2, the fitting coefficient of both Ca and Al is positive, the fitting result can be explained as no matter what the Ca/Al ratio is, the P removal degree increases with the increasing alloying concentration. Ideally, the coefficient of Ca in t_2 should be higher than that of Al. This is because with the same alloying amount under equilibrium state, Ca addition results in a lower fraction of primary Si than that of Al due to the lever law as can be seen from the eutectic point difference as shown in Fig. 7; therefore, more P segregates outside the Si and higher P removal degree achieves. However, the fitting coefficient suggests Al contributes more than that of Ca as the fitting value of Al is 0.82, and only 0.64 for Ca. Nevertheless, the fitting result is still reasonable since the cooling rate of furnace cooling becomes slower at a lower temperature. Hence, the increase of Al concentration effectively reduces the alloy liquidus results in longer solidification time, which makes Al addition becomes more beneficial on the impurity diffusion and segregation under furnace cooling.

Eventually, the obtained regression formula by PLSR can be transformed from the standardized equation and written as:

$$\eta_P = 51.76 + 10.64X_{Ca} + 2.18X_{Al} \left(1.11 < X_{Ca} < 3.16 \text{and} 0.86 < X_{Al} < 2.85 in mol\%\right) \tag{13}$$

The comparison of predicted data through PLSR and measurement is found with a good agreement and presented in Fig. 7.

3.6. Thermodynamic modelling

Even though mathematical methods indirectly provide information of the role of Ca and Al in the alloying-leaching refining process, thermodynamic modelling describes the effect of each alloying element with a more direct profile and better prediction extensionality. According to the P removal prediction model, the estimated first-order interaction coefficient of Ca and Al to P can be fitted using the obtained leaching results. It is worth noting that in order to obtain better integral accuracy in the high concentration region, the interaction coefficient formulism proposed by Ma [60] is adopted instead of the conventionally used the Wagner-Lupis-Elliott [61] or Bale-Pelton [62] formulism. Thus, the activity coefficient of P in the Si-Ca-Al liquid ($\gamma_{P \text{ in } Si-Ca-Al(l)}$) is written as:

$$\begin{aligned}\ln\gamma_{\mathrm{P\ in\ Si{-}Ca{-}Al}(l)} &= \ln\gamma^{0}_{\mathrm{P\ in\ Si}(l)} + \ln\gamma_{Si} + \varepsilon^{\mathrm{P}}_{\mathrm{P}}\ln\left(1-x_{\mathrm{P\ in\ Si}(l)}\right)\\ &- \varepsilon^{\mathrm{P}}_{\mathrm{Ca}}x_{\mathrm{Ca\ in\ Si}(l)}\left[1+\frac{\ln\left(1-x_{\mathrm{Ca\ in\ Si}(l)}\right)}{x_{\mathrm{Ca\ in\ Si}(l)}}-\frac{1}{1-x_{\mathrm{P\ in\ Si}(l)}}\right]\\ &- \varepsilon^{\mathrm{P}}_{\mathrm{Al}}x_{\mathrm{Al\ in\ Si}(l)}\left[1+\frac{\ln\left(1-x_{\mathrm{Al\ in\ Si}(l)}\right)}{x_{\mathrm{Al\ in\ Si}(l)}}-\frac{1}{1-x_{\mathrm{P\ in\ Si}(l)}}\right]\\ &+ \varepsilon^{\mathrm{P}}_{\mathrm{Ca}}x_{\mathrm{Ca\ in\ Si}(l)}{}^{2}x_{\mathrm{P\ in\ Si}(l)}\left[\frac{1}{1-x_{\mathrm{P\ in\ Si}(l)}}+\frac{1}{1-x_{\mathrm{Ca\ in\ Si}(l)}}+\frac{x_{\mathrm{P\ in\ Si}(l)}}{\left(1-x_{\mathrm{P\ in\ Si}(l)}\right)^{2}}-1\right]\\ &+ \varepsilon^{\mathrm{P}}_{\mathrm{Al}}x_{\mathrm{Al\ in\ Si}(l)}{}^{2}x_{\mathrm{P\ in\ Si}(l)}\left[\frac{1}{1-x_{\mathrm{P\ in\ Si}(l)}}+\frac{1}{1-x_{\mathrm{Al\ in\ Si}(l)}}+\frac{x_{\mathrm{P\ in\ Si}(l)}}{\left(1-x_{\mathrm{P\ in\ Si}(l)}\right)^{2}}-1\right]\end{aligned} \tag{14}$$

where $\gamma^{0}_{\mathrm{P\ in\ Si}(l)}$ represents the activity coefficient of P in liquid Si at infinite dilution, and γ_{Si} represents the activity coefficient of solvent Si, which is close to unity and can be neglected. $\varepsilon^{\mathrm{P}}_{\mathrm{P}}$, $\varepsilon^{\mathrm{P}}_{\mathrm{Ca}}$, and $\varepsilon^{\mathrm{P}}_{\mathrm{Al}}$represent the first order interaction coefficients. X_{Me} represents the concentration of doping metal Me in Si melt.

Since the P concentration in our case is only around 10 ppm, thus, the $x_{\mathrm{P\ in\ Si}(l)}$ term is neglectable. As a result, Eq. (14) is simplified as:

$$\ln\gamma_{\mathrm{P\ in\ Si{-}Ca{-}Al}(l)} = \ln\gamma^{0}_{\mathrm{P\ in\ Si}(l)} - \varepsilon^{\mathrm{P}}_{\mathrm{Ca}}\ln\left(1-x_{\mathrm{Ca\ in\ Si}(l)}\right) - \varepsilon^{\mathrm{P}}_{\mathrm{Al}}\ln\left(1-x_{\mathrm{Al\ in\ Si}(l)}\right) \tag{15}$$

It can be seen that when the alloy concentration $x_{\mathrm{Ca\ in\ Si}(l)}$ and $x_{\mathrm{Al\ in\ Si}(l)}$ are small enough, the Ma formulism is consistent with the linear composition-dependent Wagner-Lupis-Elliott or Bale-Pelton formulism. Subsequently, the segregation coefficient of P in our Si-Ca-Al alloy system, $k^{\mathrm{Si-Ca-Al}}_{\mathrm{P}}$, can be expressed by Eq. (15) (derivation is given in the Appendix).

$$k^{\mathrm{Si-Ca-Al}}_{\mathrm{P}} = k^{\mathrm{Si}}_{\mathrm{P}}\left[\left(1-x_{\mathrm{Ca\ in\ Si}(l)}\right)^{-\varepsilon^{\mathrm{P}}_{\mathrm{Ca}}}\left(1-x_{\mathrm{Al\ in\ Si}(l)}\right)^{-\varepsilon^{\mathrm{P}}_{\mathrm{Al}}}\right] \tag{16}$$

And,

$$k^{\mathrm{Si-Ca-Al}}_{\mathrm{P}} = k^{\mathrm{Si}}_{\mathrm{P}}\left[\left(1-\frac{x^{initial}_{\mathrm{Ca\ in\ Si}(l)}}{1-f_s}\right)^{-\varepsilon^{\mathrm{P}}_{\mathrm{Ca}}}\left(1-\frac{x^{initial}_{\mathrm{Al\ in\ Si}(l)}}{1-f_s}\right)^{-\varepsilon^{\mathrm{P}}_{\mathrm{Al}}}\right] \tag{17}$$

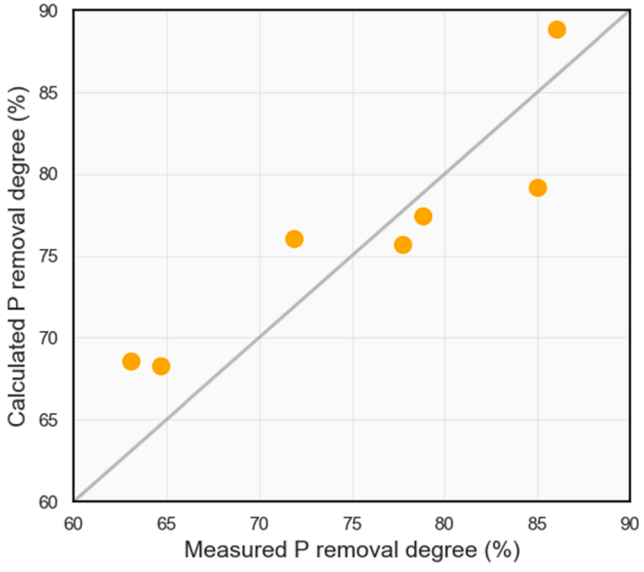

Fig. 8. Comparison between calculated and measured P removal degree of Si-Ca-Al alloys according to PLS regression.

Thus, the final P removal model is written as below based on Gulliver-Scheil solidification described before [14,15], where the detailed modelling derivation can be seen from the Appendix.

$$\eta = \left(1-\frac{1-\frac{X^{Eu}_{P\ in\ Si(l)}}{X^{initial}_{P\ in\ Si(l)}}\left(1-f^{Eu}_{s}\right)}{f^{Eu}_{s}}\right)\times 100\% \tag{18}$$

where f^{Eu}_{s} is the solidification fraction when the ternary eutectic reaction starts, and the term $\frac{X^{Eu}_{\mathrm{P\ in\ Si}(l)}}{X^{initial}_{\mathrm{P\ in\ Si}(l)}}$ is the ratio between the P concentration in the liquid droplet at the eutectic point and the initial P concentration, which can be calculated below:

$$\ln\frac{X^{Eu}_{\mathrm{P\ in\ Si}(l)}}{X^{initial}_{\mathrm{P\ in\ Si}(l)}} = \int_{0}^{f^{Eu}_{s}}\frac{1-k^{\mathrm{Si}}_{\mathrm{P}}\left[\left(1-\frac{x^{initial}_{\mathrm{Ca\ in\ Si}(l)}}{1-f_s}\right)^{-\varepsilon^{\mathrm{P}}_{\mathrm{Ca}}}\left(1-\frac{x^{initial}_{\mathrm{Al\ in\ Si}(l)}}{1-f_s}\right)^{-\varepsilon^{\mathrm{P}}_{\mathrm{Al}}}\right]}{1-f_s}df_s \tag{19}$$

The P removal degree in the Si-Ca-Al ternary alloying-leaching refining system can be therefore calculated through the model derived above. Likewise, the interaction coefficient ε^{P}_{Ca} and ε^{P}_{Al} can be fitted through the P removal model as well. By inputting the dataset of the above seven Si-Ca-Al alloys, the fitted value of $\varepsilon^{\mathrm{P}}_{\mathrm{Ca}}$ and $\varepsilon^{\mathrm{P}}_{\mathrm{Al}}$is obtained as $\varepsilon^{P}_{Ca} = -19.2$ and $\varepsilon^{\mathrm{P}}_{\mathrm{Al}} = -1.8$. The variation of R-square depends on different interaction coefficient combinations is also presented in Fig. 8, which is calculated using the Eq. (20).

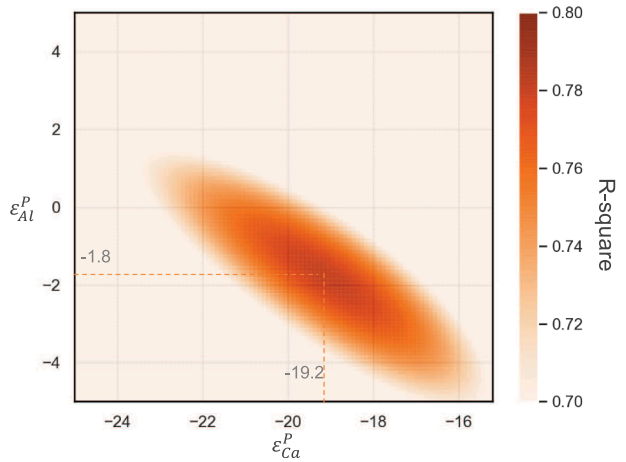

Fig. 9. Variation of R-square value with different combinations of ε^{P}_{Ca} and ε^{P}_{Al}.

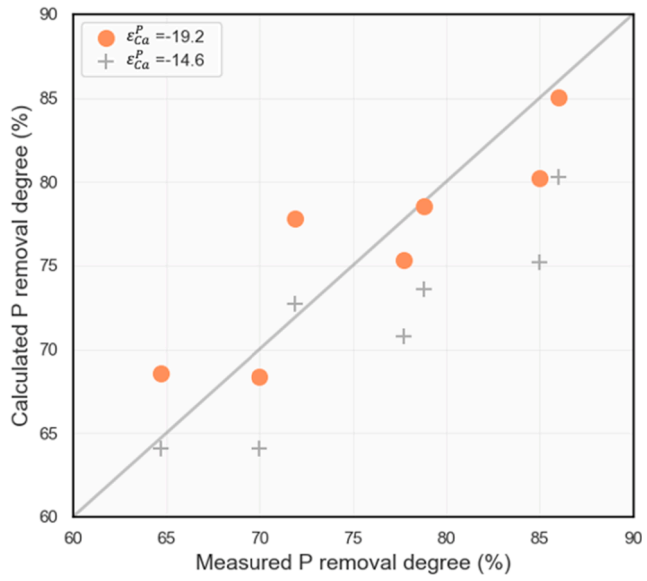

Fig. 10. Comparison between calculated and measured P removal degree of studied Si-Ca-Al alloys.

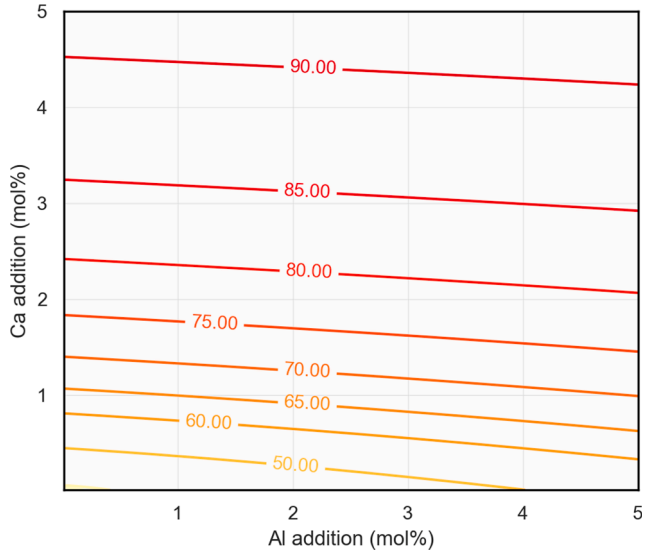

Fig. 11. Predicted P removal degree with varying Ca and Al addition of the Si-Ca-Al alloying-leaching system.

$$R^2 = 1 - \frac{\sum_i \left(\hat{y}_i - y_i\right)^2}{\sum_i \left(\bar{y}_i - y_i\right)^2} \tag{20}$$

where y_i represents the measured data, $\hat{y}_i$ represents calculated data, and $\bar{y}_i$ is the mean of dataset.

A trend can be seen from Fig. 9 that, generally, more negative ε_{Ca}^{P} corresponds to increasing ε_{Al}^{P} during the fitting process. However, the sign of ε_{Al}^{P} is mostly located in the negative region. Thus, it is speculated the interaction between Al and P is most likely to be week attraction. To further evaluate the model validity, the comparison between predicted P removal using the fitted value and measured data is shown in Fig. 10 where good accuracy can be observed over the whole range. It also worth noting that the fitted value of ε_{Ca}^{P} is more negative than the measured result $\varepsilon_{Ca}^{P} = -14.6 \pm 1.7$ by Shimpo et al.[14] at 1450 °C. One important reason for this slight difference is because the temperature effect is not considered in the current model due to the ultra-low P content. On the other side, if the impurity thermodynamic properties are not independent of temperature, the fitting result will incorporate the temperature effect, therefore, it can be regarded as an average value during the whole solidification temperature range.

The *iso*-removal curve of P is presented as Fig. 11 through the developed model. Thus, how the alloying of silicon by Ca and Al affects the leaching purification performance can be further examined. Following the increase of Al concentration, the P removal degree is only slightly increasing. However, if with fixed Al concentration, the increase of Ca addition leads to significant improvement of the P removal. Furthermore, the predicted *iso*-P removal curve also shows the consistency with the measured results that the enhancement of P removal can be achieved via increasing the overall Ca + Al alloying concentration and increasing Ca/Al mixing ratio (the slope of a line passes the origin point). Additionally, it is also seen that the contamination from alumina crucible is harmful to the P removal in a large extent due to the Ca consumption and Al substitution.

3.7. Assessment of the role of $CaAl_2Si_2$ in P removal

In the previous discussion, Ca concentration in the liquid phase has been found as the main driving force for P segregation, however, the role of $CaAl_2Si_2$ becomes much more elusive as it is frequently detected with the highest P concentration among the precipitates. In fact, the state of P at several ppm level in Si alloy still unknown as it could be either a solid solution or phosphide precipitate. It is speculated that P with such trace amount may not meet the energy requirements for the formation of a single phosphide phase. Additionally, if new phosphide forms, the newly created interface would also lead to a higher total energy state. However, it still lacks evidence for the assumption. Thus, for the first time, the possibility of P behaviour as the solute atom in solid solution of $CaAl_2Si_2$ and $CaSi_2$ was examined by first-principle calculations.

In the Si-Ca-Al alloying refining system, the potential P solid solution types are considered as below:

$$CaAl_2Si_2 + xP = Ca(Al_{2-x}P_x)Si_2 + xAl \tag{21}$$

$$CaAl_2Si_2 + xP = CaAl_2(Si_{2-x}P_x) + xSi \tag{22}$$

$$CaAl_2Si_2 + xP = (Ca_{1-x}P_x)Al_2Si_2 + xCa \tag{23}$$

$$CaSi_2 + xP = Ca(Si_{2-x}P_x) + xSi \tag{24}$$

$$CaSi_2 + xP = (Ca_{1-x}P_x)Si_2 + xCa \tag{25}$$

For convenience, the configurations chosen to evaluate the stability of P substituted solid solution were established based on the supercell $Ca_{12}Al_{24}Si_{24}$ and $Ca_{12}Si_{24}$, which are presented in Fig. 12 together with the calculated total energy via static DFT calculations. Additionally, the enthalpy changes of the corresponding solid solution reactions were also evaluated as the free energy G ($G = H$- TS) can be presented by enthalpy H at 0 K, results are listed in Table 7.

It can be seen that in $CaAl_2Si_2$, P substitution for Si (P_{Si}) is the most energy favorable, and the relative total energy order is $E(P_{Si}) < E(P_{Al}) < E0 < E(P_{Ca})$. In CaSi2, similar trend is found as $E(P_{Si}) < E0 < E(P_{Ca})$, while the structural stability order is $Ca_{12}(Si_{23}P) > Ca_{12}Si_{24} > (Ca_{11}P)Si_{24}$. By looking at the enthalpy changes, it is clearly seen that in $CaAl_2Si_2$, the process of P substitutes Si and Al atoms should be spontaneously, and the P_{Si} substitution possess exhibits higher possibility than P_{Al} substitution, while the P_{Ca} substitution is unlikely to happen. In $CaSi_2$, it is similar to the analysis of the $CaAl_2Si_2$, the Si site in preferable to be replaced by P but the Ca site cannot. Thus, the solubility of P in $CaAl_2Si_2$ and $CaSi_2$ is verified as energetically favourable and thermodynamically stable. Moreover, by comparing the enthalpy change values of $CaAl_2Si_2$ and $CaSi_2$, it suggests that P substitutional solid solution is

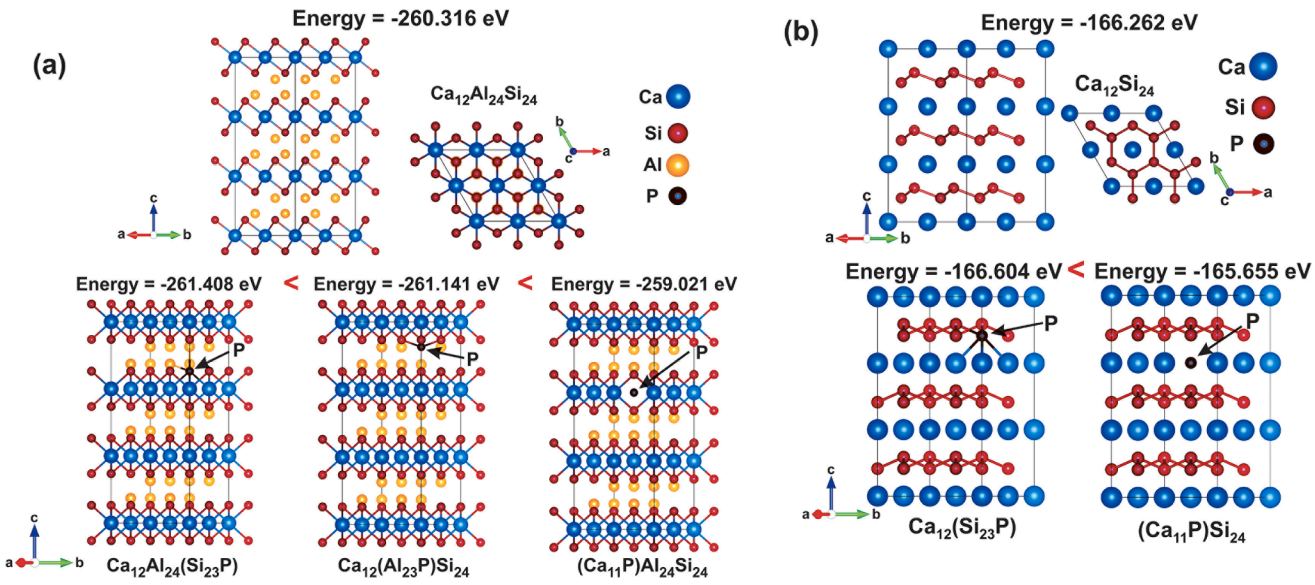

Fig. 12. Configuration and total energy of (a) supercell $Ca_{12}Al_{24}Si_{24}$ and P element substituted cell $Ca_{12}Al_{24}(Si_{23}P)$, $Ca_{12}(Al_{23}P)Si_{24}$, and $(Ca_{11}P)Al_{24}Si_{24}$; (b) supercell $Ca_{12}Si_{24}$ and P element substituted cell $Ca_{12}(Si_{23}P)$, and $(Ca_{11}P)Si_{24}$.

Table 7
Substitutional solid solution types and the corresponding enthalpy change of reactions by DFT calculations.

Matrix	Solid solution type	Substitution reaction	Enthalpy change
$CaAl_2Si_2$	$Ca_{12}(Al_{23}P)Si_{24}$	$CaAl_2Si_2 + 0.083P = CaAl_{1.917}P_{0.083}Si_2 + 0.083Al$	$\Delta H_{P_{Al}} = -0.069eV$
	$Ca_{12}Al_{24}(Si_{23}P)$	$CaAl_2Si_2 + 0.083P = CaAl_2P_{0.083}Si_{1.917} + 0.083Si$	$\Delta H_{P_{Si}} = -0.090eV$
	$(Ca_{11}P)Al_{24}Si_{24}$	$CaAl_2Si_2 + 0.083P = Ca_{0.917}Al_2P_{0.083}Si_2 + 0.083Ca$	$\Delta H_{P_{Ca}} = 0.110eV$
$CaSi_2$	$Ca_{12}(Si_{23}P)$	$CaSi_2 + 0.083P = CaP_{0.083}Si_{1.917} + 0.083Si$	$\Delta H_{P_{Si}} = -0.029eV$
	$(Ca_{11}P)Si_{24}$	$CaSi_2 + 0.083P = Ca_{0.917}P_{0.083}Si_2 + 0.083Ca$	$\Delta H_{P_{Ca}} = 0.051eV$

easier to form in $CaAl_2Si_2$ than in $CaSi_2$. Therefore, the puzzle why the $CaAl_2Si_2$ contains higher P concentration becomes clearer and explainable. The reasons are two folds, firstly, as P tends to segregate into the liquid phase, and $CaAl_2Si_2$ precipitation closes to the end stage of solidification, where the P content is already enriched before the nucleation of $CaAl_2Si_2$. Secondly, the high P solubility of the $CaAl_2Si_2$ phase further benefits the P dissolution and brings it as the precipitates with the higher P content. It is also seen that the role of $CaAl_2Si_2$ phase is not decisive for the P segregation improvement, which is essentially related more to the alloying elements concentration and their interaction with P in the liquid phase.

It should be noted that even though the present work provides evidence to support the solid solution mechanism, however, the above discussions may be only restricted to low P concentration at several ppm-level. This is because, in reality, the mechanism for P removal should be manifold, coexisting, and even competitive between each other. For instance, if the initial P concentration increases to higher amount at hundreds or thousands ppm-level, the formation and precipitation of phosphide may become the main mechanism for P removal. Moreover, when dealing with even higher P concentration or slower solidification kinetics, the effect of P evaporation should also play an important role in the P removal from Si.

4. Conclusions

In the present work, a series of Si-Ca-Al alloys were studied for Si purification. The role of alloy composition and the ternary $CaAl_2Si_2$ phase in the Si alloying-leaching process was further investigated with the focus on P removal. The main conclusions are summarized below:

1. Alumina crucible is not recommended for the Si-Ca alloy preparation as it will contaminate the alloy and reduce the final P removal degree.
2. P removal degree is found to increase with increasing Ca/Al mixing ratio and increasing total alloying amount (Ca + Al).
3. Ca concentration exhibits a strongly positive and monotonic relationship to P removal via statistical analyses, while there is no strong attraction interaction found between Al and P.
4. A model was established for the prediction of P removal degree in the Si-Ca-Al refining system based on the Gulliver-Scheil solidification and thermodynamics approach. The averaged interaction coefficients between P and Ca, Al are fitted as $\varepsilon_{Ca}^{P} = -19.2$ and $\varepsilon_{Al}^{P} = -1.8$, which further confirms Ca concentration in liquid phase is the essential driving force for P segregation.
5. The formation of P solid solution was verified by first-principle simulations. $CaAl_2Si_2$ exhibits higher P solubility than the $CaSi_2$ phase, which further explains the reason for the high P concentration observed in $CaAl_2Si_2$.

CRediT authorship contribution statement

Mengyi Zhu: Conceptualization, Investigation, Visualization, Writing - original draft. **Shengying Yue:** Software, Investigation, Writing - review & editing. **Guixuan Wu:** Software, Investigation, Writing - review & editing. **Kai Tang:** Software, Methodology. **Yijiang Xu:** Methodology, Writing - review & editing. **Jafar Safarian:** Conceptualization, Methodology, Supervision, Project administration, Writing - review & editing.

Declaration of Competing Interest

The authors declare that they have no known competing financial interests or personal relationships that could have appeared to influence the work reported in this paper.

Acknowledgment

This work was performed at NTNU within the Research Centre for Sustainable Solar Cell Technology (FME SuSolTech, project number 257639), co-sponsored by the Norwegian Research Council and industry partners. The authors also appreciate the ICP-MS assistance by Gagan Paudel from NTNU.

Appendix A

The chemical potential of P between the primary crystallized Si and liquid phase are identical at equilibrium:

$$\mu_{\mathrm{P\ in\ Si}(s)} = \mu_{\mathrm{P\ in\ Si-Ca-Al}(l)} \tag{A1}$$

Above equation can be expressed in term of activity:

$$\Delta G^{*}_{\mathrm{P\ in\ Si}(s)} + RTlna_{\mathrm{P\ in\ Si}(s)} = \Delta G^{*}_{\mathrm{P\ in\ Si-Ca-Al}(l)} + \mathrm{RTln}a_{\mathrm{P\ in\ Si-Ca-Al}(l)} \tag{A2}$$

And,

$$\Delta G^{*fus}_{P\ in\ dilute\ alloy} = \mathrm{RTln}\left(\frac{a_{\mathrm{P\ in\ Si}(s)}}{a_{\mathrm{P\ in\ Si-Ca-Al}(l)}}\right) = \mathrm{RTln}\left(k_{\mathrm{P}}^{\mathrm{Si-Ca-Al}}\frac{\gamma_{\mathrm{P\ in\ Si}(s)}}{\gamma_{\mathrm{P\ in\ Si-Ca-Al}(l)}}\right) \tag{A3}$$

where ΔG_P^{*fus} is the Gibbs energy of P fusion in between the two phases.

Considering the Gibbs energy and activity coefficient are functions of state, as presented in Fig. A1, Eq. (A4) and Eq. (A5) are obtained:

$$\Delta G^{*fus}_{P\ in\ Si} = \Delta \mathrm{G}_{1(\mathrm{P},s)} + \Delta G_P^{*fus} + \Delta \mathrm{G}_{2(\mathrm{P},l)} \tag{A4}$$

$$\Delta G^{*fus}_{P\ in\ dilute\ alloy} = \Delta \mathrm{G}_{1(\mathrm{P},s)} + \Delta G_P^{*fus} + \Delta \mathrm{G}_{3(\mathrm{P},l)} \tag{A5}$$

where -$\Delta \mathrm{G}_{1(\mathrm{P},s)}$, $\Delta \mathrm{G}_{2(\mathrm{P},l)}$, and $\Delta \mathrm{G}_{3(\mathrm{P},l)}$ are the Gibbs energy of P pure substance dissolution in the corresponding dilute systems, and ΔG_P^{*fus} is the Gibbs energy of fusion of P pure substance.

Since the P concentration is extremely low in our studied system, the difference of liquid phase dissolution energy of P in Si and Si dilute alloy is considered insignificant, thus, it yields:

$$\Delta \mathrm{G}_{2(\mathrm{P},l)} \approx \Delta \mathrm{G}_{3(\mathrm{P},l)} \tag{A6}$$

And,

$$\Delta G^{*fus}_{P\ in\ Si} = \Delta G^{*fus}_{P\ in\ dilute\ alloy} = \Delta G_P^{*fus} \tag{A7}$$

Therefore, we have:

$$k_{\mathrm{P}}^{\mathrm{Si-Ca-Al}} = exp\left(\frac{\Delta G_P^{*fus}}{RT}\right)\frac{\gamma_{\mathrm{PinSi-Ca-Al}(l)}}{\gamma_{\mathrm{PinSi}(s)}} \tag{A8}$$

And for the infinite dilute P in Si,

$$k_{\mathrm{P}}^{\mathrm{Si}} = exp\left(\frac{\Delta G_P^{*fus}}{RT}\right)\frac{\gamma^0_{\mathrm{P\ in\ Si}(l)}}{\gamma^0_{\mathrm{P\ in\ Si}(s)}} \tag{A9}$$

Introducing the $\gamma^0_{\mathrm{PinSi}(l)}$ term to Eq, (A8):

$$k_{\mathrm{P}}^{\mathrm{Si-Ca-Al}} = exp\left(\frac{\Delta G_P^{*fus}}{RT}\right)\frac{\gamma^0_{\mathrm{P\ in\ Si}(l)}}{\gamma_{\mathrm{P\ in\ Si}(s)}}\frac{\gamma_{\mathrm{P\ in\ Si-Ca-Al}(l)}}{\gamma^0_{\mathrm{P\ in\ Si}(l)}} \tag{A10}$$

Since the alloy concentration in solid Si is neglectable, thus:

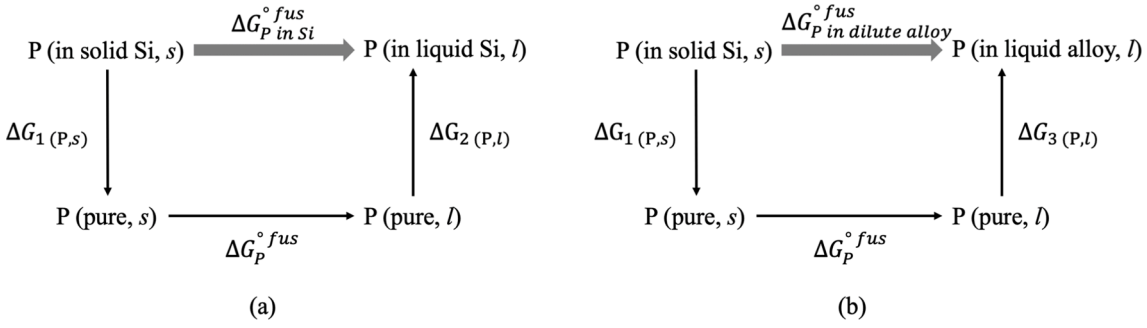

Fig. A1. Illustration of the states of P transformation in (a) pure Si and (b) dilute Si alloy.

$$\gamma_{\mathrm{P\ in\ Si}(s)} = \gamma^{0}_{\mathrm{P\ in\ Si}(s)} \tag{A11}$$

Subsequently, introducing the Eq. (A11) back to Eq. (A10):

$$k_{\mathrm{P}}^{\mathrm{Si-Ca-Al}} = k_{\mathrm{P}}^{\mathrm{Si}} \frac{\gamma_{\mathrm{P\ in\ Si-Ca-Al}(l)}}{\gamma^{0}_{\mathrm{P\ in\ Si}(l)}} \tag{A12}$$

Conventionally, the Wagner-Lupis-Elliot or Bale-Pelton formulism are applied to describe the relationship between the activity coefficient. Considering at the end stage of solidification, the concentration of alloying element in the remaining liquid phase may be high enough that the first order of interaction coefficient is not adequate to describe, thus, the formulism proposed by Zhongting Ma is adopted:

$$\begin{aligned}\ln\gamma_{\mathrm{P\ in\ Si-Ca-Al}(l)} =& \ln\gamma^{0}_{\mathrm{P\ in\ Si}(l)} + \ln\gamma_{Si} + \varepsilon^{\mathrm{P}}_{\mathrm{P}}\ln\left(1 - x_{\mathrm{P\ in\ Si}(l)}\right) - \varepsilon^{\mathrm{P}}_{\mathrm{Ca}} x_{\mathrm{Ca\ in\ Si}(l)}\left[1 + \frac{\ln\left(1 - x_{\mathrm{Ca\ in\ Si}(l)}\right)}{x_{\mathrm{Ca\ in\ Si}(l)}} - \frac{1}{1 - x_{\mathrm{P\ in\ Si}(l)}}\right] \\ & - \varepsilon^{\mathrm{P}}_{\mathrm{Al}} x_{\mathrm{Al\ in\ Si}(l)}\left[1 + \frac{\ln\left(1 - x_{\mathrm{Al\ in\ Si}(l)}\right)}{x_{\mathrm{Al\ in\ Si}(l)}} - \frac{1}{1 - x_{\mathrm{P\ in\ Si}(l)}}\right] + \varepsilon^{\mathrm{P}}_{\mathrm{Ca}} x_{\mathrm{Ca\ in\ Si}(l)}{}^{2} x_{\mathrm{P\ in\ Si}(l)}\left[\frac{1}{1 - x_{\mathrm{P\ in\ Si}(l)}} + \frac{1}{1 - x_{\mathrm{Ca\ in\ Si}(l)}} + \frac{x_{\mathrm{P\ in\ Si}(l)}}{\left(1 - x_{\mathrm{P\ in\ Si}(l)}\right)^{2}} - 1\right] \\ & + \varepsilon^{\mathrm{P}}_{\mathrm{Al}} x_{\mathrm{Al\ in\ Si}(l)}{}^{2} x_{\mathrm{P\ in\ Si}(l)}\left[\frac{1}{1 - x_{\mathrm{P\ in\ Si}(l)}} + \frac{1}{1 - x_{\mathrm{Al\ in\ Si}(l)}} + \frac{x_{\mathrm{P\ in\ Si}(l)}}{\left(1 - x_{\mathrm{P\ in\ Si}(l)}\right)^{2}} - 1\right]\end{aligned} \tag{A13}$$

The $x_{\mathrm{P\ in\ Si}(l)}$ term is ignored due to the concentration of P is at only around 10 ppm level in the studied system:

$$\ln\gamma_{\mathrm{P\ in\ Si-Ca-Al}(l)} = \ln\gamma^{0}_{\mathrm{P\ in\ Si}(l)} - \varepsilon^{\mathrm{P}}_{\mathrm{Ca}}\ln\left(1 - x_{\mathrm{Ca\ in\ Si}(l)}\right) - \varepsilon^{\mathrm{P}}_{\mathrm{Al}}\ln\left(1 - x_{\mathrm{Al\ in\ Si}(l)}\right) \tag{A14}$$

Thus, by introducing Eqs. (A14) to (A12), the segregation coefficient $k_{\mathrm{P}}^{\mathrm{Si-Ca-Al}}$ can be expressed as:

$$k_{\mathrm{P}}^{\mathrm{Si-Ca-Al}} = k_{\mathrm{P}}^{\mathrm{Si}}\left[\left(1 - x_{\mathrm{Ca\ in\ Si}(l)}\right)^{-\varepsilon^{\mathrm{P}}_{\mathrm{Ca}}}\left(1 - x_{\mathrm{Al\ in\ Si}(l)}\right)^{-\varepsilon^{\mathrm{P}}_{\mathrm{Al}}}\right] \tag{A15}$$

In order to obtain the function of the degree of P removal from the P segregation coefficient in Si-Ca-Al liquid phase, we start from the definition of the degree of P removal:

$$\eta = \left(\frac{X^{initial}_{\mathrm{P\ in\ Si}(l)} - \overline{X}_{\mathrm{P\ in\ Si(s)}}}{X^{initial}_{\mathrm{P\ in\ Si}(l)}}\right) \times 100\% \tag{A16}$$

where $\overline{X}_{\mathrm{PinSi(s)}}$ is the averaged concentration of P inside primary Si, and can be obtained from the integration from solidification starting point to the eutectic reaction starting point as:

$$\overline{X}_{\mathrm{P\ in\ Si(s)}} f_s^{Eu} = \int_0^{f_s^{Eu}} X_{\mathrm{P\ in\ Si}(s)}\, df_s \tag{A17}$$

And,

$$X_{\mathrm{P\ in\ Si}(s)} = k_P^{\mathrm{Si-Ca-Al}} X^{initial}_{\mathrm{P\ in\ Si}(l)}\left(1 - f_s\right)^{k_P^{\mathrm{Si-Ca-Al}} - 1} \tag{A18}$$

Thus, we have:

$$\overline{X}_{\mathrm{P\ in\ Si(s)}} = \frac{X^{initial}_{\mathrm{P\ in\ Si}(l)}}{f_s^{Eu}}\left(1 - \left(1 - f_s^{Eu}\right)^{k_{\mathrm{P}}^{\mathrm{Si-Ca-Al}}}\right) \tag{A19}$$

Similarly,

$$X^{Eu}_{\mathrm{P\ in\ Si}(l)} = X^{initial}_{\mathrm{P\ in\ Si}(l)}\left(f_s^{Eu}\right)^{k_{\mathrm{P}}^{\mathrm{Si-Ca-Al}} - 1} \tag{A20}$$

Thus, the expression of P removal degree can be transformed as Eq. (A21):

$$\eta = \left(1 - \frac{1 - \frac{X^{Eu}_{P\ in\ Si(l)}}{X^{initial}_{P\ in\ Si(l)}}\left(1 - f_s^{Eu}\right)}{f_s^{Eu}}\right) \times 100\% \tag{A21}$$

In order to obtain the expression of the term $\frac{X^{Eu}_{P\ in\ Si(l)}}{X^{initial}_{P\ in\ Si(l)}}$, the Gulliver-Scheil equation should be considered:

$$(1 - f_s)dX_{\mathrm{P}(l)} = \left(X_{\mathrm{P}(l)} - X_{\mathrm{P}(s)}\right)df_{\mathrm{s}} \tag{A22}$$

Considering the relationship $X_{\mathrm{P}(s)} = k_{\mathrm{P}}^{\mathrm{Si-Ca-Al}} X_{\mathrm{P}(l)}$ and after integration, it yields following Eq. (A23):

$$\ln\frac{X^{Eu}_{\mathrm{P\ in\ Si}(l)}}{X^{initial}_{\mathrm{P\ in\ Si}(l)}} = \int_0^{f_s^{Eu}} \frac{1 - k_{\mathrm{P}}^{\mathrm{Si-Ca-Al}}}{1 - f_s} df_{\mathrm{s}} \tag{A23}$$

Combine Eq. (A15), we finally obtain the Eq. (A24), which can be solved numerically:

$$\ln\frac{X_{P\ in\ Si(l)}^{Eu}}{X_{P\ in\ Si(l)}^{initial}}=\int_0^{f_s^{Eu}}\frac{1-k_P^{Si}\left[\left(1-\frac{x_{Ca\ in\ Si(l)}^{initial}}{1-f_s}\right)^{-\varepsilon_{Ca}^{P}}\left(1-\frac{x_{Al\ in\ Si(l)}^{initial}}{1-f_s}\right)^{-\varepsilon_{Al}^{P}}\right]}{1-f_s}df_s \tag{A24}$$

References

[1] Renewables 2020 Global Status Report, Paris, 2020. https://www.ren21.net/reports/global-status-report/ (accessed November 15, 2020).

[2] S. Pizzini, Towards solar grade silicon: Challenges and benefits for low cost photovoltaics, Sol. Energy Mater. Sol. Cells. 94 (2010) 1528–1533, https://doi.org/10.1016/J.SOLMAT.2010.01.016.

[3] L.K. Jakobsson, M. Tangstad, Thermodynamics of Boron Removal from Silicon Using CaO-MgO-Al2O3-SiO2 Slags, Metall. Mater. Trans. B Process Metall. Mater. Process. Sci. 49 (2018) 1699–1708, https://doi.org/10.1007/s11663-018-1250-7.

[4] Z. Wang, Z. Ge, J. Liu, G. Qian, B. Du, The mechanism of boron removal from silicon alloy by electric field using slag treatment, Sep. Purif. Technol. 199 (2018) 134–139, https://doi.org/10.1016/j.seppur.2018.01.055.

[5] Y. Wang, K. Morita, Reaction Mechanism and Kinetics of Boron Removal from Molten Silicon by CaO–SiO2–CaCl2 Slag Treatment, J. Sustain. Metall. 1 (2015) 126–133, https://doi.org/10.1007/s40831-015-0015-7.

[6] J. Safarian, G. Tranell, M. Tangstad, Boron Removal from Silicon by CaO-Na2O-SiO2 Ternary Slag, Metall. Mater. Trans. E. 2 (2015) 109–118, https://doi.org/10.1007/s40553-015-0048-7.

[7] Y. Li, L. Zhang, Application of Si-Based Solvents to the Purification of Metallurgical Grade-Silicon, Sep. Purif. Rev. (2019) 1–24, https://doi.org/10.1080/15422119.2019.1623253.

[8] L.T. Khajavi, K. Morita, T. Yoshikawa, M. Barati, Removal of Boron from Silicon by Solvent Refining Using Ferrosilicon Alloys, Metall. Mater. Trans. B Process Metall. Mater. Process. Sci. 46 (2014) 615–620, https://doi.org/10.1007/s11663-014-0236-3.

[9] L. Huang, H. Lai, C. Lu, M. Fang, W. Ma, P. Xing, J. Li, X. Luo, Enhancement in extraction of boron and phosphorus from metallurgical grade silicon by copper alloying and aqua regia leaching, Hydrometallurgy. 161 (2016) 14–21, https://doi.org/10.1016/j.hydromet.2016.01.013.

[10] L. Tafaghodi Khajavi, M. Barati, Thermodynamics of Phosphorus in Solvent Refining of Silicon Using Ferrosilicon Alloys, Metall. Mater. Trans. B Process Metall. Mater. Process. Sci. 48 (2017) 268–275, https://doi.org/10.1007/s11663-016-0804-9.

[11] Y. Lei, P. Qiu, K. Chen, X. Chen, W. Ma, J. Wu, K. Wei, S. Li, G. Lv, J. Qiu, Mechanism of ZrB2 formation in Al-Si alloy and application in Si purification, ACS Sustain. Chem. Eng. 7 (2019) 12990–12996, https://doi.org/10.1021/acssuschemeng.9b02065.

[12] B. Ban, X. Bai, J. Li, Y. Li, J. Chen, S. Dai, The Mechanism of P Removal by Solvent Refining in Al-Si-P System, Metall. Mater. Trans. B Process Metall. Mater. Process. Sci. 46 (2015) 2430–2437, https://doi.org/10.1007/s11663-015-0449-0.

[13] T. Yoshikawa, K. Morita, An Evolving Method for Solar-Grade Silicon Production: Solvent Refining, JOM. 64 (2012) 946–951, https://doi.org/10.1007/s11837-012-0371-8.

[14] T. Shimpo, T. Yoshikawa, K. Morita, Thermodynamic study of the effect of calcium on removal of phosphorus from silicon by acid leaching treatment, Metall. Mater. Trans. B. 35 (2004) 277–284, https://doi.org/10.1007/s11663-004-0029-1.

[15] M. Zhu, A. Azarov, E. Monakhov, K. Tang, J. Safarian, Phosphorus separation from metallurgical-grade silicon by magnesium alloying and acid leaching, Sep. Purif. Technol. 240 (2020), 116614, https://doi.org/10.1016/j.seppur.2020.116614.

[16] M.D. Johnston, M. Barati, Calcium and titanium as impurity getter metals in purification of silicon, Sep. Purif. Technol. 107 (2013) 129–134, https://doi.org/10.1016/j.seppur.2013.01.028.

[17] Y. Lei, W. Ma, G. Lv, K. Wei, S. Li, K. Morita, Purification of metallurgical-grade silicon using zirconium as an impurity getter, Sep. Purif. Technol. 173 (2017) 364–371, https://doi.org/10.1016/j.seppur.2016.09.051.

[18] Y. Lei, W. Ma, X. Ma, J. Wu, K. Wei, S. Li, K. Morita, Leaching behaviors of impurities in metallurgical-grade silicon with hafnium addition, Hydrometallurgy. 169 (2017) 433–439.

[19] M. Zhu, D. Wan, K. Tang, J. Safarian, Impurity removal from Si by Si-Ca-Mg ternary alloying-leaching system, Mater. Des. (2020), 109348, https://doi.org/10.1016/j.matdes.2020.109348.

[20] J. Safarian, M. Tangstad, Vacuum refining of molten silicon, Metall. Mater. Trans. B Process Metall. Mater. Process. Sci. 43 (2012) 1427–1445, https://doi.org/10.1007/s11663-012-9728-1.

[21] A. Hoseinpur, K. Tang, J. Safarian, Kinetic study of vacuum evaporation of elements from ternary melts; case of dilute solution of P in Si-Al melts, Sep. Purif. Technol. 235 (2020), https://doi.org/10.1016/j.seppur.2019.116284.

[22] S.-S. Zheng, T. Abel Engh, M. Tangstad, X.-T. Luo, Separation of Phosphorus from silicon by induction vacuum refining, Sep. Purif. Technol. 82 (2011) 128–137, https://doi.org/10.1016/j.seppur.2011.09.001.

[23] A. Hoseinpur, J. Safarian, Vacuum refining of Si at ulra-high temperatures, Vacuum. (2021), 109924, https://doi.org/10.1016/J.VACUUM.2020.109924.

[24] J. Safarian, K. Tang, K. Hildal, G. Tranell, Boron Removal from Silicon by Humidified Gases, Metall. Mater. Trans. E. 1 (2014) 41–47, https://doi.org/10.1007/s40553-014-0007-8.

[25] Ø.S. Sortland, M. Tangstad, Boron Removal from Silicon Melts by H2O/H2 Gas Blowing: Mass Transfer in Gas and Melt, Metall. Mater. Trans. E. 1 (2014) 211–225, https://doi.org/10.1007/s40553-014-0021-x.

[26] G. Qian, L. Sun, H. Chen, Z. Wang, K. Wei, W. Ma, Enhancing impurities removal from Si by controlling crystal growth in directional solidification refining with Al–Si alloy, J. Alloys Compd. 820 (2020), 153300, https://doi.org/10.1016/j.jallcom.2019.153300.

[27] H. Chen, K. Morita, X. Ma, Z. Chen, Y. Wang, Boron removal for solar-grade silicon production by metallurgical route: A review, Sol. Energy Mater. Sol. Cells. 203 (2019), 110169, https://doi.org/10.1016/j.solmat.2019.110169.

[28] J. Wu, Y. Zhou, W. Ma, M. Xu, B. Yang, Synergistic Separation Behavior of Boron in Metallurgical Grade Silicon Using a Combined Slagging and Gas Blowing Refining Technique, Metall. Mater. Trans. B Process Metall. Mater. Process. Sci. 48 (2017) 22–26, https://doi.org/10.1007/s11663-016-0860-1.

[29] Z. Xia, J. Wu, W. Ma, Y. Lei, K. Wei, Y. Dai, Separation of boron from metallurgical grade silicon by a synthetic CaO-CaCl2 slag treatment and Ar-H2O-O2 gas blowing refining technique, Sep. Purif. Technol. 187 (2017) 25–33, https://doi.org/10.1016/j.seppur.2017.06.037.

[30] J. Li, P. Cao, P. Ni, Y. Li, Y. Tan, Enhanced boron removal from metallurgical grade silicon by the slag refining method with the addition of tin, Sep. Sci. Technol. 51 (2016) 1–6, https://doi.org/10.1080/01496395.2016.1165702.

[31] D. Zhao, Y. Li, Revealing the factors influencing grain boundary segregation of P, As in Si: Insights from first-principles, Acta Mater. 168 (2019) 52–62, https://doi.org/10.1016/j.actamat.2019.02.014.

[32] F.A. Trumbore, Solid Solubilities of Impurity Elements in Germanium and Silicon, Bell Syst. Tech. J. 39 (1960) 205–233, https://doi.org/10.1002/j.1538-7305.1960.tb03928.x.

[33] I. Obinata, N. Komatsu, A study on purification of metallurgical grade silicon by Si-Al alloy, Sci. Rep. RITU 9 (9) (1957) 118.

[34] T. Yoshikawa, K. Morita, Removal of phosphorus by the solidification refining with Si-Al melts, Sci. Technol. Adv. Mater. 4 (2003) 531–537, https://doi.org/10.1016/j.stam.2003.12.007.

[35] Y. Li, B. Ban, J. Li, T. Zhang, X. Bai, J. Chen, S. Dai, Effect of Cooling Rate on Phosphorus Removal During Al-Si Solvent Refining, Metall. Mater. Trans. B. 46 (2015) 542–544, https://doi.org/10.1007/s11663-015-0291-4.

[36] B. Ban, X. Bai, J. Li, J. Chen, S. Dai, Effect of kinetics on P removal by Al-Si solvent refining at low solidification temperature, J. Alloys Compd. 685 (2016) 604–609, https://doi.org/10.1016/j.jallcom.2016.05.312.

[37] J.L. Gumaste, B.C. Mohanty, R.K. Galgali, U. Syamaprasad, B.B. Nayak, S.K. Singh, P.K. Jena, Solvent refining of metallurgical grade silicon, Sol. Energy Mater. 16 (1987) 289–296, https://doi.org/10.1016/0165-1633(87)90077-3.

[38] H. Xue, G. Lv, W. Ma, D. Chen, J. Yu, Separation Mechanism of Primary Silicon from Hypereutectic Al-Si Melts Under Alternating Electromagnetic Fields, Metall. Mater. Trans. A. (n.d.). http://doi.org/10.1007/s11661-015-2889-1.

[39] Y. Xu, Y. Deng, D. Casari, R.H. Mathiesen, X. Liu, Y. Li, Revealing the nucleation kinetics of primary Si particles in hypereutectic Al–Si alloys under the influence of P inoculation, J. Mater. Sci. 55 (2020) 15621–15635, https://doi.org/10.1007/s10853-020-05095-3.

[40] Y. Xu, Y. Deng, D. Casari, R.H. Mathiesen, X. Liu, Y. Li, Growth kinetics of primary Si particles in hypereutectic Al-Si alloys under the influence of P inoculation: Experiments and modelling, J. Alloys Compd. 854 (2021), 155323, https://doi.org/10.1016/j.jallcom.2020.155323.

[41] A. Schei, High Purity Silicon Production, in: Int. Semin. Refin. Alloy. Liq. Alum. Ferro-Alloys, Trondheim, Norway, 1985.

[42] L. Huang, A. Danaei, S. Thomas, P. Xing, J. Li, X. Luo, M. Barati, Solvent extraction of phosphorus from Si-Cu refining system with calcium addition, Sep. Purif. Technol. 204 (2018) 205–212, https://doi.org/10.1016/J.SEPPUR.2018.04.087.

[43] H. Lai, L. Huang, C. Lu, M. Fang, W. Ma, P. Xing, J. Li, X. Luo, Leaching behavior of impurities in Ca-alloyed metallurgical grade silicon, Hydrometallurgy. 156 (2015) 173–181, https://doi.org/10.1016/j.hydromet.2015.06.012.

[44] H. Sakiani, S.H. Tabaian, J. Chen, Effect of calcium addition on the silicon purification in the presence of low concentration of iron, J. Alloys Compd. 830 (2020), 154112, https://doi.org/10.1016/j.jallcom.2020.154112.

[45] J.C. Anglézio, C. Servant, F. Dubrous, Characterization of metallurgical grade silicon, J. Mater. Res. 5 (1990) 1894–1899, https://doi.org/10.1557/JMR.1990.1894.

[46] T. Margaria, J. Anglezio, C. Servant, Intermetallic compounds in metallurgical silicon, in: Proc. 6th Int. Ferroalloys Congr., Cape Town, 1992: pp. 209–214. https://www.pyro.co.za/InfaconVI/1209-Margaria.pdf.

[47] L. Hu, Z. Wang, X. Gong, Z. Guo, H. Zhang, Purification of metallurgical-grade silicon by Sn-Si refining system with calcium addition, Sep. Purif. Technol. 118 (2013) 699–703, https://doi.org/10.1016/j.seppur.2013.08.013.
[48] L. Sun, Z. Wang, H. Chen, D. Wang, G. Qian, Removal of Phosphorus in Silicon by the Formation of CaAl2Si2 Phase at the Solidification Interface, Metall. Mater. Trans. B Process Metall. Mater. Process. Sci. 48 (2017) 420–428, https://doi.org/10.1007/s11663-016-0848-x.
[49] H. Lai, Z. Sheng, J. Li, P. Xing, X. Luo, Enhanced separation of phosphorus from metallurgical grade silicon by CaAl2Si2 phase reconstruction, Sep. Purif. Technol. 191 (2018) 257–265, https://doi.org/10.1016/j.seppur.2017.09.034.
[50] C. Zhang, H. Lai, Y. Zhang, Z. Sheng, J. Li, P. Xing, X. Luo, Extraction of phosphorus from metallurgical grade silicon using a combined process of Si-Al-Ca solvent refining and CaO-CaF2 slag treatment, Sep. Purif. Technol. 232 (2020), 115954, https://doi.org/10.1016/j.seppur.2019.115954.
[51] G. Kresse, J. Furthmüller, Efficiency of ab-initio total energy calculations for metals and semiconductors using a plane-wave basis set, Comput. Mater. Sci. 6 (1996) 15–50, https://doi.org/10.1016/0927-0256(96)00008-0.
[52] G. Kresse, J. Furthmüller, Efficient iterative schemes for ab initio total-energy calculations using a plane-wave basis set, Phys. Rev. B - Condens. Matter Mater. Phys. 54 (1996) 11169–11186, https://doi.org/10.1103/PhysRevB.54.11169.
[53] P.E. Blöchl, Projector augmented-wave method, Phys. Rev. B. 50 (1994) 17953–17979, https://doi.org/10.1103/PhysRevB.50.17953.
[54] J.P. Perdew, K. Burke, M. Ernzerhof, Generalized gradient approximation made simple, Phys. Rev. Lett. 77 (1996) 3865–3868, https://doi.org/10.1103/PhysRevLett.77.3865.
[55] H. Usui, K. Kuroki, First principles study on the thermoelectric performance of 122-type Zintl phase compounds, J. Phys. Scoiety Janpan. 89 (2020) 1–11, https://doi.org/10.7566/JPSJ.89.124707.
[56] H. Sakiani, S.H. Tabaian, J. Chen, Influence of interactions between alumina crucible and Si-Ca-Fe melt on B and P removal from silicon, Sep. Purif. Technol. 255 (2021), 117743, https://doi.org/10.1016/j.seppur.2020.117743.
[57] S. Cui, M. Paliwal, I.-H. Jung, Thermodynamic Optimization of Ca-Fe-Si System and Its Applications to Metallurgical Grade Si-Refining Process, (n.d.). http://doi.org/10.1007/s40553-014-0010-0.
[58] M. Zhu, S.Y. Yue, K. Tang, J. Safarian, New Insights into Silicon Purification by Alloying-Leaching Refining: A Comparative Study of Mg–Si, Ca–Si, and Ca–Mg–Si Systems, ACS Sustain. Chem. Eng. 8 (2020) 15953–15966, https://doi.org/10.1021/acssuschemeng.0c05564.
[59] Y. Marot, A. Correia-Anacleto, D. Jocelyn Le, Preparing silane compound, by reacting silicide/silicon alloy in form of powder, in presence of calcium chloride, with hydrochloric acid that is pre-dissolved in aqueous solution, where silane is useful in manufacture of e.g. solar cell, 2012.
[60] Z. Ma, Thermodynamic description for concentrated metallic solutions using interaction parameters, 2001. http://doi.org/10.1007/s11663-001-0011-0.
[61] C.H.P. Lupis, Chemcial thermodynamics of materials, Elsevier Science Publishing Co., Inc., 1983.
[62] C.W. Bale, A.D. Pelton, The Unified Interaction Parameter Formalism: Thermodynamic Consistency and Applications, Metall. Mater. Trans. A. 21A (1989).